Multidisciplinary Design Optimization of Low-Boom Supersonic Aircraft with Mission Constraints

Wu Li[*] and Karl Geiselhart[†]

NASA Langley Research Center, Hampton, Virginia 23681, USA

Conceptual design of low-boom supersonic aircraft is heavily dictated by aircraft volume and lift distributions. These unique design characteristics make it a challenge to enforce mission requirements (such as static margins and trim requirements) during design optimization. This low-boom design challenge is resolved by using reversed equivalent area targets for low-fidelity low-boom inverse design and a block coordinate optimization (BCO) method for multidisciplinary design optimization (MDO). The corresponding low-boom MDO problem includes aircraft mission constraints on ranges, cruise speeds, trim for low-boom cruise, static margins for takeoff/cruise/landing, takeoff/landing field lengths, approach velocity, and tail rotation angles for trim at takeoff/landing, as well as fuselage volume constraints for passengers and main gear storage. The BCO method is developed to optimally resolve the conflicts between the low-boom inverse design objective and other design constraints. This method is successfully applied to design a low-boom supersonic configuration that carries 40 passengers, flies a low-boom mission with cruise Mach of 1.6 and range of 2,500 nm, and cruises overwater at Mach 1.8 with range of 3,600 nm. The generated configuration satisfies all specified mission constraints and has the potential to match a reversed equivalent area target with ground noise level below 70 PLdB.

Nomenclature

A_e = any equivalent area (ft^2) including $A_{e,m}$, $A_{e,LoFi}$, $A_{e,CFD}$, $A_{e,r}$, and their lift/volume parts

$A_{e,CFD}$ = $A_{e,m}$ (ft^2) calculated using computational fluid dynamics (CFD) lift distribution

$A_{e,LoFi}$ = $A_{e,m}$ (ft^2) calculated using low-fidelity aero lift distribution

$A_{e,m}$ = classical equivalent area (ft^2) defined by Mach angle cut method

$A_{e,r}$ = reversed equivalent area (ft^2) defined by using reverse propagation of CFD off-body pressure

$A_{e,LoFi}^{lift}$ = lift part (ft^2) of $A_{e,LoFi} = A_{e,LoFi}^{lift} + A_e^{volume}$

$A_{e,CFD}^{lift}$ = lift part (ft^2) of $A_{e,CFD} = A_{e,CFD}^{lift} + A_e^{volume}$

$A_{e,r}^{target}$ = $A_{e,r}$ target (ft^2) for configuration defined by $\boldsymbol{D}$

$A_{e,r,0}^{target}$ = $A_{e,r}$ target (ft^2) for baseline defined by $\boldsymbol{D}_0$

A_e^{volume} = volume part (ft^2) of $A_{e,LoFi} = A_{e,LoFi}^{lift} + A_e^{volume}$ or $A_{e,CFD} = A_{e,CFD}^{lift} + A_e^{volume}$

c_i = chord length (ft) of airfoil at span location y_i

c_{root} = chord length (ft) of root airfoil of horizontal tail

c_{tip} = chord length (ft) of tip airfoil of horizontal tail

$\boldsymbol{D}$ = design vector of fuselage parameters, wing parameters, horizontal tail parameters, engine thrust, and auxiliary parameters for takeoff and landing

$\boldsymbol{D}_{HiF}$ = design vector for supersonic configuration with low ground noise level when analyzed using CFD off-body pressure for sonic boom propagation

$\boldsymbol{D}_{LoF}$ = design vector for supersonic configuration satisfying $f(\boldsymbol{D}_{LoF}) \leq 0.015 \cdot A_{e,LoFi}(l_e, \boldsymbol{D}_{LoF})$

$\boldsymbol{D}_{LoW}$ = design vector for the lowest weight solution on Pareto frontier of multiobjective MDO that satisfies $f(\boldsymbol{D}_{LoW}) \leq 0.015 \cdot A_{e,LoFi}(l_e, \boldsymbol{D}_{LoW})$

$\boldsymbol{D}_0$ = design vector for baseline configuration

d_i = width parameter (ft) for fuselage cross section at x_i

f = inverse design objective function for low-fidelity low-boom front shaping

---

[*] Senior Research Engineer, Aeronautics Systems Analysis Branch
[†] Aerospace Engineer, Aeronautics Systems Analysis Branch

American Institute of Aeronautics and Astronautics

g_i	=	mission constraint function for low-boom MDO
i	=	index
$\boldsymbol{l}$	=	lower bound vector for $\boldsymbol{D}$
l_{e}	=	effective length (ft) for configuration defined by $\boldsymbol{D}$, which is the largest effective distance where Mach angle cut plane intersects the configuration
$l_{\mathrm{e},0}$	=	effective length (ft) for baseline defined by $\boldsymbol{D}_0$
$\mathrm{MTOGW_{fea}}$	=	maximum takeoff gross weight estimate from FEA-based analysis
$\mathrm{MTOGW_{flops}}$	=	maximum takeoff gross weight estimate from FLOPS weight analysis
s_i	=	sectional span length (ft) of i-th wing section
$\boldsymbol{u}$	=	upper bound vector for $\boldsymbol{D}$
W_0	=	weight at the start of cruise (lb) for baseline defined by $\boldsymbol{D}_0$
W_{crs}	=	weight at the start of cruise (lb) for configuration defined by $\boldsymbol{D}$
$W_{\mathrm{fuse,fea}}$	=	fuselage weight estimate from FEA-based analysis
$W_{\mathrm{fuse,flops}}$	=	fuselage weight estimate from FLOPS weight analysis
$W_{\mathrm{wing,fea}}$	=	wing structural weight estimate from FEA-based analysis
$W_{\mathrm{wing,flops}}$	=	wing structural weight estimate from FLOPS weight analysis
x, y, z	=	coordinates (ft) of point in space
x_{aft}	=	x coordinate (ft) of trailing edge of root airfoil of wing
x_{e}	=	effective distance (ft) for A_{e} calculation
$x_{\mathrm{e,mr}}$	=	effective distance location (ft) satisfying $|A_{\mathrm{e,CFD}}(x_{\mathrm{e}}) - A_{\mathrm{e,r}}(x_{\mathrm{e}})| \leq \varepsilon_{\mathrm{mr}}$ for $x_{\mathrm{e}} \leq x_{\mathrm{e,mr}}$
x_{frt}	=	x coordinate (ft) of leading edge of root airfoil of wing
x_i	=	x coordinate (ft) of fuselage cross section location
x_{tip}	=	x coordinate (ft) of trailing edge of tip airfoil of wing
y_i	=	y coordinate (ft) of span location of wing
$\delta_{i,\mathrm{max}}$	=	camber-line designation, fraction of chord from leading edge over which design load is uniform, for NACA 63-series airfoil at span location y_i
δ_{max}	=	camber-line designation, fraction of chord from leading edge over which design load is uniform, for NACA 63-series airfoil
ε	=	error tolerance of $0.015 \cdot A_{\mathrm{e,LoFi}}(l_{\mathrm{e}},\boldsymbol{D})$ for low-boom inverse design objective $f(\boldsymbol{D})$
$\varepsilon_{\mathrm{mr}}$	=	error tolerance for $|A_{\mathrm{e,CFD}}(x_{\mathrm{e}}) - A_{\mathrm{e,r}}(x_{\mathrm{e}})|$
θ_{htail}	=	deflection angle (degree) of an all-moving horizontal tail at cruise
θ_i	=	twist angle (degree) of airfoil at span location y_i
λ	=	$l_{\mathrm{e}} \cdot \lambda_0/l_{\mathrm{e},0}$, upper limit (ft) to compute front A_{e} matching error for configuration defined by $\boldsymbol{D}$
λ_0	=	upper limit (ft) to compute front A_{e} matching error for baseline defined by $\boldsymbol{D}_0$
μ	=	estimate of ratio $A_{\mathrm{e,r}}(l_{\mathrm{e}})/A_{\mathrm{e,CFD}}(l_{\mathrm{e}})$ for expected CFD-based low-boom design
$\tau_{i,\mathrm{max}}$	=	design section lift coefficient for NACA 63-series airfoil at span location y_i
τ_{max}	=	design section lift coefficient for NACA 63-series airfoil
ω_{fuse}	=	calibration factor for FLOPS fuselage weight estimate
ω_{wing}	=	calibration factor for FLOPS wing structural weight estimate

I. Introduction

DESIGN of low-boom supersonic aircraft is heavily dictated by aircraft volume and lift distributions. Because lift distributions from low-fidelity aerodynamics and computational fluid dynamics (CFD) are significantly different, it is necessary to use CFD for low-boom design. An integrated design optimization process of using CFD analysis to reduce the initial shock pressure rise of sonic boom ground signature can be found in Ref. [1]. Automation of Euler CFD analysis has been successfully completed for aircraft conceptual design [2-4]. Euler CFD analysis is routinely used for analysis and design of low-boom supersonic configurations [5]. CFD-based low-boom inverse design methods can be successfully applied to reduce the undertrack ground noise level of a supersonic configuration to approximately 78 PLdB [6-10] and the Cart3D adjoint low-boom inverse design method has the potential to reduce the ground noise level further [11,12]. However, for any realistic design of supersonic aircraft, it is necessary to include other design objectives and/or mission constraints [13-38].

In theory, the low-boom characteristics of a supersonic aircraft are very sensitive to its outer mold line (OML) and surface pressure distribution at cruise. Any significant alteration of its OML (including control surface deflections) at cruise could have a detrimental effect on its low-boom characteristics. Tables 5 and 6 in Ref. [39] quantify the variability of the perceived loudness of ground noise due to the control surface deflections during cruise flight of a

low-boom flight demonstrator. For a well-designed low-boom configuration, it is generally necessary to use fuel to maintain level flight with the designed low-boom OML instead of control surface deflections. This leads to one of the most difficult design constraints for low-boom supersonic aircraft: positioning the aerodynamic center of pressure such that it can be trimmed with the available center of gravity (CG) range from fuel redistribution at cruise. This trim constraint for low-boom supersonic aircraft is also largely determined by the aircraft volume and lift distributions. Methods were developed to incorporate the trim constraint in the low-boom target for reversed equivalent area ($A_{e,r}$) [6] and they were used successfully for CFD-based design of two low-boom supersonic configurations [8,9]. However, these methods are computationally too expensive and not applicable during preliminary conceptual design when mission constraints are included in optimization. A conceptual design approach of incorporating the trim constraint in the low-boom F-function target of a wing-body configuration [40] needs to be further verified by using an aircraft configuration with nacelles and tails. In this paper, a block coordinate optimization (BCO) method for low-boom multidisciplinary design optimization (MDO) is proposed to generate a low-boom supersonic concept that has the potential to match a low-boom target with ground noise level below 70 PLdB and satisfies twelve mission constraints including the trim constraint for low-boom cruise.
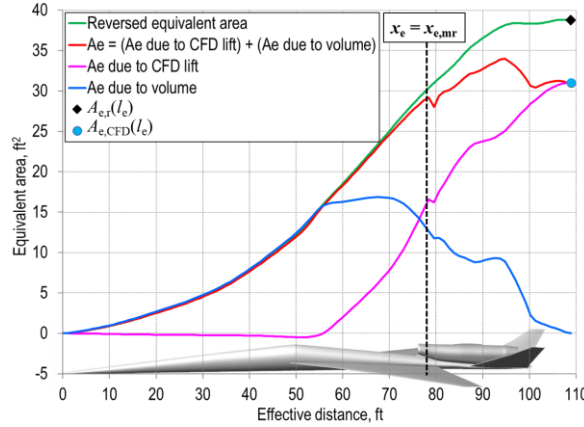

Fig. 1 Comparison of $A_{e,\text{CFD}}$ and $A_{e,r}$.

As the low-boom design technology evolves over time, it becomes clear that the classical low-boom design methods for A_e matching (see Ref. [41] and references therein) cannot shape the aft ground signature because $A_{e,m}(l_e)$ is significantly lower than $A_{e,r}(l_e)$ calculated from CFD off-body pressure distribution. Note the difference of $A_{e,r}(l_e)$ and $A_{e,\text{CFD}}(l_e)$ of a 100 ft low-boom supersonic demonstrator concept in Fig. 1, which is a superposition of Figs. 9 and 10 in Ref. [9]. Classical A_e targets cannot be used for CFD-based low-boom design. Here a CFD-based low-boom design means a configuration with a low ground noise level when analyzed using CFD off-body pressure for sonic boom propagation. The method of increasing the value of an $A_{e,m}$ target at $x_e = l_e$ for low-boom inverse design was applied to design of a low-boom supersonic business jet and two low-boom wind tunnel models [13,42] and was also used for design of a Mach 1.7 scaled supersonic experimental airplane [43] without considering the aft shape of the ground signature. The most advanced $A_{e,m}$ matching method [41] using CFD lift analysis and the generalized sonic-boom minimization theory can match a wing-body configuration to an $A_{e,m}$ target that has a ground signature with a flat-top front shape and an N-wave aft shape. But this type of method is not applicable to any supersonic configuration that cannot be treated as a body of revolution for sonic boom analysis (*i.e.*, any configuration with nacelles).

Analysis using CFD off-body pressure indicates that $|A_{e,\text{CFD}}(x_e) - A_{e,r}(x_e)| \leq \varepsilon_{mr}$ for $x_e \leq x_{e,mr}$ with a small error tolerance ε_{mr} and an $x_{e,mr}$ location in the aft part of the wing before the nacelles (see Fig. 1). That is, the classical sonic boom minimization theory of treating a supersonic configuration as a body of revolution is valid up to the aft part of the wing. The required value of $A_{e,r}^{\text{target}}(l_e)$ for CFD-based low-boom inverse design is $\mu \cdot A_{e,m}(l_e)$, where the scaling factor $\mu > 1$ is *a priori* estimate of $A_{e,r}(l_e,\boldsymbol{D}_{\text{HiF}})/A_{e,\text{CFD}}(l_e,\boldsymbol{D}_{\text{HiF}})$ for a CFD-based low-boom design $\boldsymbol{D}_{\text{HiF}}$. The use of $A_{e,r}^{\text{target}}$ for $A_{e,m}$-based low-boom front shaping leads to a possible decomposition of a CFD-based low-boom inverse design problem into three subproblems: (i) matching $A_{e,\text{LoFi}}$ with $A_{e,r}^{\text{target}}$ for $x_e \leq x_{e,mr}$, (ii) matching $A_{e,r}$ with $A_{e,r}^{\text{target}}$ for $x_e \leq x_{e,mr}$ using minor wing modifications, and (iii) matching $A_{e,r}$ with $A_{e,r}^{\text{target}}$ for $x_e \geq x_{e,mr}$ with modifications of the aft components. This decomposition approach is motivated by the three approximation equations in the following formula: $A_{e,r}^{\text{target}}(x_e) \approx A_{e,\text{LoFi}}(x_e,\boldsymbol{D}_{\text{LoF}}) = A_e^{\text{volume}}(x_e,\boldsymbol{D}_{\text{LoF}}) + A_{e,\text{LoFi}}^{\text{lift}}(x_e,\boldsymbol{D}_{\text{LoF}}) \approx A_e^{\text{volume}}(x_e,\boldsymbol{D}_{\text{HiF}}) + A_{e,\text{CFD}}^{\text{lift}}(x_e,\boldsymbol{D}_{\text{HiF}}) = A_{e,\text{CFD}}(x_e,\boldsymbol{D}_{\text{HiF}}) \approx A_{e,r}(x_e,\boldsymbol{D}_{\text{HiF}})$ for $x_e \leq x_{e,mr}$. Here $\boldsymbol{D}_{\text{LoF}}$ is the low-fidelity low-boom front shaping solution and $\boldsymbol{D}_{\text{HiF}}$ is the final CFD-based low-boom design. The first approximation equation is a result of the low-fidelity low-boom front

American Institute of Aeronautics and Astronautics

shaping. Preliminary numerical results indicate that minor wing modifications to D_{LoF} can yield a high-fidelity design D_{HiF} such that $A_{\text{e,CFD}}^{\text{lift}}(x_\text{e},D_{\text{HiF}}) \approx A_{\text{e,LoFi}}^{\text{lift}}(x_\text{e},D_{\text{LoF}})$ for $x_\text{e} \leq x_{\text{e,mr}}$. The minor wing modifications also imply that $A_\text{e}^{\text{volume}}(x_\text{e},D_{\text{HiF}}) \approx A_\text{e}^{\text{volume}}(x_\text{e},D_{\text{LoF}})$. So, the 2nd approximation equation holds. The last approximation equation follows from the definition of $x_{\text{e,mr}}$. In other words, the low-fidelity low-boom shaping can largely determine the front shape of a CFD-based low-boom design if $A_{\text{e,r}}^{\text{target}}$ is used for low-fidelity low-boom inverse design. So, if the total error of $A_{\text{e,LoFi}}(x_\text{e}) - A_{\text{e,r}}^{\text{target}}(x_\text{e})$ for $x_\text{e} \leq x_{\text{e,mr}}$ is used as the low-boom inverse design objective function, then the generated low-fidelity low-boom design has a front shape close to a CFD-based low-boom design and is a good initial design for CFD-based low-boom inverse design optimization.

In this paper, the A_e matching error for low-fidelity low-boom front shaping is used as an objective function in conceptual design of low-boom supersonic transports. The resulting MDO problem with mission constraints is solved using a multidisciplinary feasible (MDF) architecture [44], where the disciplinary couplings are enforced for analyses of a supersonic configuration. Previous low-boom MDO studies [24-38] used either loudness or maximum magnitude of sonic boom ground signature as the low-boom design objective function. Unfortunately, no design study shows that minimization of loudness or maximum magnitude of sonic boom ground signature could reduce the noise of the ground signature below 79 PLdB. In contrast, CFD-based low-boom inverse design methods [6-12] can generate supersonic configurations with CFD-based sonic boom ground signatures below 79 PLdB. Using the low-fidelity low-boom inverse design objective in low-boom MDO is the first step to enable CFD-based low-boom inverse design optimization in low-boom MDO of supersonic transports.

In theory, if the design space contains a configuration that satisfies the specified mission constraints, then any direct optimization problem with the specified mission constraints has an optimal solution; while an inverse design optimization problem with the same mission constraints might have no desirable solution. This is due to the implicit requirement on an optimal solution of any inverse design optimization problem: the optimized inverse design objective value must be close to the ideal objective value of zero. This makes the low-boom MDO with the low-boom inverse design objective much more difficult to solve than any low-boom MDO using a direct optimization objective. In this paper, the proposed BCO method is applied to solve a multiobjective MDO problem with an inverse design objective for low-boom front shaping, another design objective for minimum weight, and the specified mission constraints.

The paper is organized as follows. Section II documents the formulation of the multiobjective low-boom MDO problem and BCO. In Section III, the proposed BCO method is applied to design a low-boom low-weight supersonic transport satisfying the specified mission constraints. The final section includes the concluding remarks.

II.   Block Coordinate Optimization Method for Low-Boom MDO

In practice, an MDO solution process for aircraft conceptual design requires tremendous efforts to set up. The data links among different disciplinary analysis codes are complex, and the data consistency is difficult to verify. Moreover, empirical design knowledge is necessary for many implicit assumptions used to define the MDO problem. It is not necessary to include all the details about setting up and solving the low-boom MDO problem in this paper. In the following subsections, only the important inputs/outputs and key formulation/solution issues are discussed.

A. Baseline Geometry and Design Variables

An OpenVSP [45] baseline geometry is constructed using some empirical knowledge about low-boom supersonic transports. A parametric study of equivalent area targets shows that a supersonic configuration with a length of 242 ft has the potential to carry 40 passengers, cruise at Mach number of 1.6 and altitude of 45,000 ft, and achieve a low-boom ground noise level below 70 PLdB. This determines the fuselage length of 242 ft. The fuselage has a predetermined side shape (see Fig. 2): The front shape promotes the ground visibility for pilots even though external vision systems will likely be required; the aft shape combines the attachment need of a horizontal tail and the aft fuselage shape of Concorde (see [46] for a brief account of how Concorde evolved from a research project to a real vehicle). A cross section height of 7.3 ft is used for the passenger cabin approximately from $x = 93$ ft to 173 ft. The fuselage has 11 design variables (see the blue variables in Fig. 2) with 7 width parameters ($d_1, \ldots, d_7$) at the cross-section locations ($x_1, \ldots, x_7$) and 4 cross section location parameters (x_1, x_2, x_3, x_4).
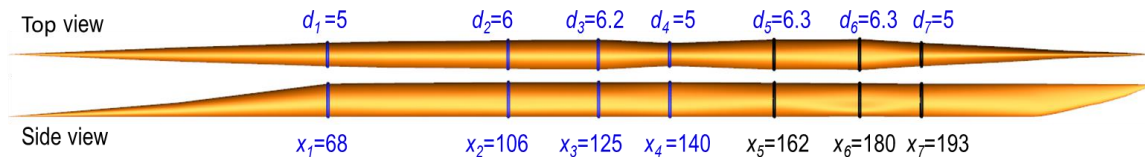

Fig. 2 Baseline fuselage OML and its parameterized cross sections.

4

American Institute of Aeronautics and Astronautics

The fuselage cross section widths are optimized while maintaining the volume for 40 passenger seats, service area, and main gear storage. The coke bottle shape for the width distribution near $x = 140$ ft (see Fig. 2) is determined by a preliminary wave drag minimization. Lower bound constraints for the seven width design variables are used to maintain the fuselage volume for passengers and main gear storage, where the lower bounds are used for the baseline.

$$d_1 \geq 5, \ d_2 \geq 6, \ d_3 \geq 6.2, \ d_4 \geq 5, \ d_5 \geq 6.3, \ d_6 \geq 6.3, \ d_7 \geq 5 \tag{1}$$

However, the width constraints depend on the cabin layout design. The constraints in Eq. (1) for d_2 and d_3 are strongly affected by the width d_4 of 5 ft for the baseline and could be relaxed if the lower bound of d_4 is higher because the layout can be modified to take advantage of the larger d_4. Small perturbation ranges for design variables x_1, x_2, x_3, and x_4 are used to make the fuselage volume distribution more flexible to help match a given low-boom $A_{e,r}$ target.
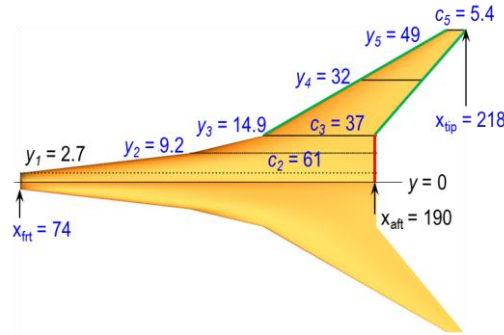
Fig. 3 Baseline wing planform and its parameterized cross sections.

The baseline wing planform in Fig. 3 is mainly determined by the lift distribution requirement for low-boom shaping (*i.e.*, it has the potential to eliminate the differences between the $A_{e,r}$ target and $A_{e,LoFi}$). The wingspan is 98 ft and the wing area is 3775 ft^2. The planform has 5 sections, with the first rectangular section hidden inside the fuselage. The longitudinal locations of the trailing edges (TE) of the three inboard sections are fixed at $x = 190$ ft. This location is determined by the main gear packaging and an attempt to shield the engine inlet shocks. The two outer wing sections form a trapezoidal shape, with an airfoil definition at the span location y_4 for more flexibility in lift tailoring. Nine design variables (see the blue variables in Fig. 3) are used to morph the baseline wing planform without creating any undesirable planform shape: x coordinate (x_{frt}) of the leading edge (LE) of the root section, x coordinate (x_{tip}) of TE of the tip airfoil, sectional spans for the four outboard sections (defined by y_i-y_{i-1}), and chord lengths at y_2, y_3, and y_5. By forcing $x_{tip} > x_{aft}$, the TE of the outboard wing section has a backward sweep. A monotone decrease of the chord lengths of the airfoils from inboard to outboard can be easily enforced with bounds on the chord lengths, which ensures the LE sweeps of wing sections are positive. These nine planform parameters define a unique wing planform under the specified shape constraints for the rectangular root section, three fixed inboard TEs, and trapezoidal shape for two outboard sections. This wing planform parametric scheme allows the use of simple bounds on the design variables to define a large design space for the wing planform that does not include any undesirable wing planform shape.

The airfoil thicknesses are based on the available empirical data. The NACA 63-series airfoils [47] are used to define the baseline wing. A camber parameter δ_{max} and design lift parameter τ_{max} (*i.e.*, the parameters A and CLI in the computer code to generate NACA 63-series airfoils [47]) are used to parameterize each airfoil. Eight parameters $\delta_{i,max}$ and $\tau_{i,max}$ for airfoils at the span locations y_i (i=1,2,3,4) are used as design variables. Moreover, the twist angles for airfoils at the span locations y_4 and y_5 are also used as design variables. A total of 10 design variables are available to modify the camber surface of a given wing planform. The inboard wing twist variables are fixed to ensure that the main gear strut can be stored inside the wing.

The highest possible angle of incidence of the wing with respect to the fuselage is used to minimize the cruise angle of attack. In general, a higher cruise angle of attack results in a shorter effective length of the configuration at cruise and makes it more difficult to attain a low-boom design. An angle of incidence of 1.4° is used for the baseline wing, which is fixed during the design optimization process.

The planform parameters of a trapezoidal horizontal tail are used as the design variables: sweep, span, root chord length, and tip chord length. The deflection angle of the all-moving horizontal tail at cruise is also used as a design variable to trade the amount of the lift carried by the tail for the weight at the start of cruise. The vertical tail is approximately sized by the lateral control requirement and the pylon is roughly sized for structural integrity. These two components are fixed during the design optimization process. The nacelle geometry is based on an advanced engine for supersonic transports and is scaled for the required thrust. Figure 4 is the baseline configuration including all geometry components and the landing gear.
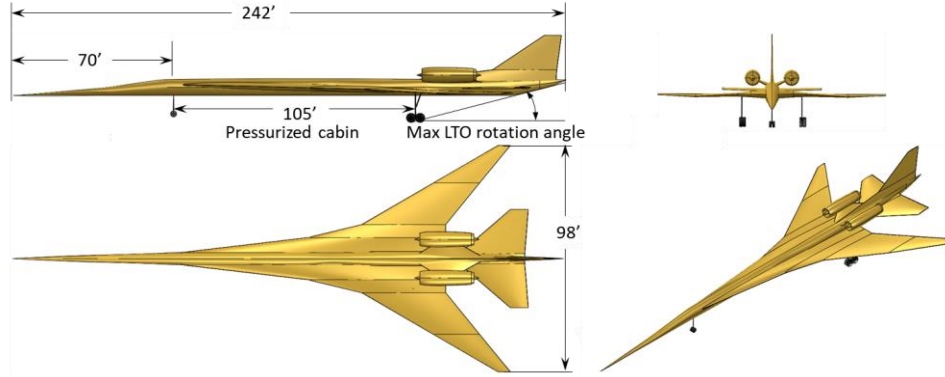
American Institute of Aeronautics and Astronautics

Fig. 4 Baseline configuration.

Table 1 Auxiliary LTO design variables for baseline

LE flap deflection angle for landing = -2°	Main gear length = 11.5 ft
TE flap deflection angle for landing = 10°	Longitudinal CG offset for takeoff = 8 ft
TE flap deflection angle for takeoff = 13.7°	Longitudinal CG offset for landing = 8 ft

Six auxiliary design variables for landing and takeoff (LTO) and their values for the baseline are listed in Table 1. These auxiliary design variables are used as control parameters to satisfy the LTO constraints. Flap sizes also affect LTO performance, but they are not used as design variables and change proportionally with wing chords in this paper. Two other important parameters related to LTO analysis are engine thrust and main gear longitudinal location. The engine thrust affects the mission analysis, engine weight, nacelle size, and LTO field lengths. The baseline has an engine thrust of 49,000 lb. The engine thrust is used as a design variable to minimize the maximum takeoff gross weight (MTOGW) in this paper. The main gear location affects the aircraft CG, LTO static margins (SM) and field lengths, and fuselage volume constraint for main gear storage. Main gear longitudinal location was a design variable during the initial layout design, but its value is fixed at 176 ft for all configurations in this paper.

Obviously, if there were an ideal low-boom design that were not included in the design space, any optimization method would fail to find such a solution. In practice, defining the design space is a knowledge-based trial and error process. The exact bounds for the design variables are not specified here, because they are subject to changes after each optimization run.

B. Equivalent Area Target Scaling for Inverse Design Objective

The prevailing low-boom optimization approach is to minimize the difference between a low-boom target and relevant $A_{e,r}$ or off-body pressure distribution of the aircraft configuration. For any given low-boom target, it is impossible to know *a priori* whether it can be matched by a configuration with a given cruise weight at a specified cruise altitude. So, it is not uncommon to find no desirable solution to the low-boom inverse design problem after repeated trials when the cruise lift constraint is imposed, or a low-boom solution is found for a significantly different cruise weight.

If the aircraft weight and CG analyses are included in low-boom inverse design, then the weight at the start of cruise changes with design modifications. A fixed MTOGW might make the low-boom design problem unnecessarily more difficult because any excess MTOGW leads to a heavier aircraft at the start of cruise, which usually means worse boom characteristics.

An additional challenge for low-fidelity low-boom inverse design arises due to the potentially significant differences between $A_{e,LoFi}$ and $A_{e,r}$, which could render the low-fidelity low-boom design completely irrelevant to the CFD-based low-boom design.

A solution to these design challenges is the use of scaled $A_{e,r}$ targets for low-fidelity low-boom inverse design optimization. For this method, assume that a baseline configuration $\boldsymbol{D}_0$ has a weight W_0 at the start of cruise (from the mission analysis) at a specified cruise altitude. First, compute its effective length $l_{e,0}$. A parametric Bezier or spline curve [48] can be used to represent the low-boom equivalent area target $A_{e,r,0}^{target}$ for the baseline. The shape parameters for $A_{e,r,0}^{target}$ are optimized to minimize the PLdB value of the ground signature generated from $A_{e,r,0}^{target}$ subject to the constraint $A_{e,r,0}^{target}(l_{e,0})/A_{e,LoFi}(l_{e,0},\boldsymbol{D}_0) = \mu$. The most reliable estimate of μ is $A_{e,r}(l_e)/A_{e,CFD}(l_e)$ of an existing CFD-based low-boom design. If no such a low-boom design is available, one could use $A_{e,r}(l_e)/A_{e,CFD}(l_e)$ of the baseline or an

6

American Institute of Aeronautics and Astronautics

empirical value of about 1.2 for supersonic transports. The value of μ used for generating $A_{\text{e,r,0}}^{\text{target}}$ is important only when CFD-based low-boom inverse design is coupled with the low-fidelity low-boom MDO. The $A_{\text{e,r}}$ target for any configuration $\boldsymbol{D}$ can be generated by the following weight scaling formula.

$$A_{\text{e,r}}^{\text{target}}(x_{\text{e}}) = \frac{W_{\text{crs}}}{W_0} \cdot A_{\text{e,r,0}}^{\text{target}}\left(\frac{l_{\text{e,0}}}{l_{\text{e}}} \cdot x_{\text{e}}\right) \tag{2}$$

Here W_{crs} and l_{e} are the weight at the start of cruise and effective length for $\boldsymbol{D}$, respectively.

Then determine an upper limit λ_0 near $x_{\text{e,mr}}$ for front A_{e} matching error calculation (see Fig. 1). To reduce the impact of the effective length change on the matching error calculation during MDO, the upper limit for calculation of the matching error between $A_{\text{e,LoFi}}$ and $A_{\text{e,r}}^{\text{target}}$ for $\boldsymbol{D}$ is updated by

$$\lambda = \frac{l_{\text{e}}}{l_{\text{e,0}}} \cdot \lambda_0 \tag{3}$$

The low-boom inverse design objective function $f(\boldsymbol{D})$ can be defined by the maximum absolute difference or integral of the squares of differences between $A_{\text{e,LoFi}}$ and $A_{\text{e,r}}^{\text{target}}$. That is,

$$f(\boldsymbol{D}) = \max_{0 \le x_{\text{e}} \le \lambda} \left| A_{\text{e,r}}^{\text{target}}(x_{\text{e}}) - A_{\text{e,LoFi}}(x_{\text{e}}) \right| \tag{4}$$

or

$$f(\boldsymbol{D}) = \left(\frac{1}{\lambda} \cdot \int_0^\lambda \left| A_{\text{e,r}}^{\text{target}}(x_{\text{e}}) - A_{\text{e,LoFi}}(x_{\text{e}}) \right|^2 dx_{\text{e}}\right)^{\frac{1}{2}} \tag{5}$$

The scaling equation Eq. (2) allows the reversed equivalent area target $A_{\text{e,r}}^{\text{target}}$ to have approximately the same effective length and end value as the $A_{\text{e,r}}$ for $\boldsymbol{D}$. In theory, $A_{\text{e,r}}^{\text{target}}(l_{\text{e}},\boldsymbol{D}) \approx A_{\text{e,r}}(l_{\text{e}},\boldsymbol{D})$ is only accurate if $\boldsymbol{D}$ is close to the baseline $\boldsymbol{D}_0$ and μ = $A_{\text{e,r}}(l_{\text{e}},\boldsymbol{D}_0)/A_{\text{e,CFD}}(l_{\text{e}},\boldsymbol{D}_0)$. In practice, it might be necessary to update μ, $l_{\text{e,0}}$, W_0, $A_{\text{e,r,0}}^{\text{target}}$, and λ_0 using the analysis results of the newly generated design during optimization iterations to improve the accuracy of $A_{\text{e,r}}^{\text{target}}(l_{\text{e}},\boldsymbol{D}) \approx A_{\text{e,r}}(l_{\text{e}},\boldsymbol{D})$ for an expected CFD-based low-boom design $\boldsymbol{D}$.

C. Multidisciplinary Feasible Architecture for Low-Boom MDO

Figure 5 is the flowchart for an MDF architecture [44] to compute the objective and constraint values for a supersonic aircraft concept. The analyses involved in the objective and constraint evaluations include propulsion, aerodynamics, aircraft weights estimation, mission and LTO performance, stability, equivalent area, sonic boom propagation, and ground signature loudness. Details for the involved analysis codes were documented in Refs. [14,49], except that the low-boom target scaling and the inverse design objective function $f(\boldsymbol{D})$ are defined in the preceding subsection.
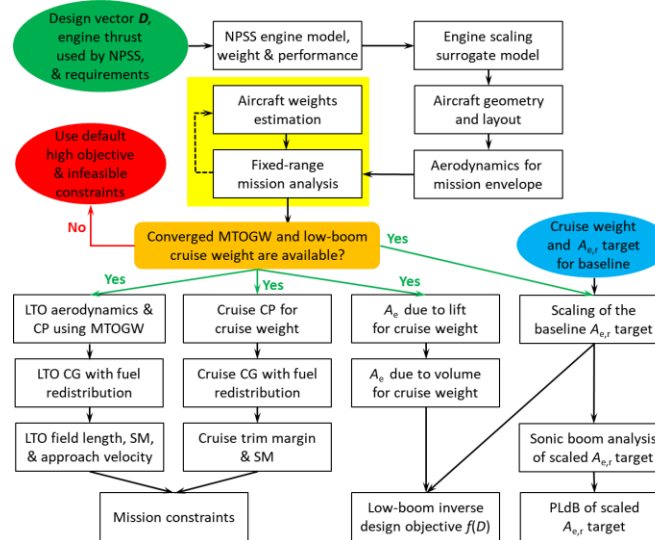

Fig. 5 MDF architecture for analysis of supersonic aircraft concept.

American Institute of Aeronautics and Astronautics

An advanced engine model was developed using the Numerical Propulsion System Simulation (NPSS) [50,51]. This engine model is only scaled based on the engine thrust in this paper. To avoid expensive runs of NPSS, the engine thrust for NPSS is always fixed and a surrogate model is used during optimization iterations. The engine sizes, weight, and performance data are linearly scaled by the surrogate model for any engine thrust in D. The optimized engine thrust in D is reanalyzed by using NPSS to validate the scaling after any optimization using the engine thrust in D as a design variable. This can be done simply by setting the engine thrust value used by NPSS to the engine thrust in D. The propulsion system performance data, used by Flight Optimization System (FLOPS) [52,53] for LTO and cruise analyses, affect the MTOGW and range. All aerodynamic data used for mission performance analyses are generated throughout the flight envelope using WINGDES [54]. For drag calculation, in addition to drag due to lift from WINGDES, skin friction drag is estimated using the method in Ref. [55] and wave drag is estimated using a modified version of the Harris far-field wave drag program [56]. Aircraft weights are computed by FLOPS [52,57]. A standard mission analysis uses MTOGW, aerodynamics data, propulsion system performance data, and component weights as the inputs, and computes the maximum range that the aircraft can fly with available fuel while satisfying the mission requirements on cruise Mach and cruise altitude. The range is an output of the standard mission analysis and a constraint must be used to satisfy each minimum range requirement. In contrast, the fixed-range mission analysis uses an iteration method implemented in FLOPS to compute the required MTOGW input for the specified range. So, the fixed-range mission analysis is the inverse of the standard mission analysis when aerodynamics data, propulsion system performance data, and component weights are fixed. The highlighted yellow iteration loop in Fig. 5 is a coupled weight and mission analysis using FLOPS for both overwater and overland missions. To start a fixed-range mission analysis, the zero-fuel weight must be specified, which is generated by the aircraft weights estimation analysis. But, one key input for the aircraft weights estimation analysis is MTOGW, which is an output of the fixed-range mission analysis. For a dual-mission analysis, two MTOGW values are generated by FLOPS and the maximum of these two values is the output of the dual-mission analysis for the FLOPS weights estimation. So, an iteration process is required to ensure that the MTOGW generated by the fixed-range mission analysis equals the MTOGW used for the aircraft weights estimation. It usually takes a few iterations to get a converged MTOGW, so the coupled weight and mission analysis can be completed efficiently. The iterations for MTOGW ensure that the range constraint is satisfied with the minimum MTOGW.

No matter which mission analysis option is used, insufficient thrust and/or poor aerodynamic performance could lead to failure of the mission analysis. The dominant failure case is insufficient thrust to climb to the required cruise altitude. The required minimum thrust depends on aerodynamic performance and MTOGW. No reasonable constraint can ensure that the coupled mission and weight analysis will generate a valid MTOGW for all configurations in the design space. For each failed case, no further analysis is required; predetermined high objective value and infeasible constraint values are used for the underlying design so that the optimization algorithm will move away from designs with failed mission analyses.

Because the low-boom signature is extremely sensitive to changes in lift distribution, trimming with deflection of an aerodynamic surface such as the all-moving horizontal tail would cause severe degradation of the low-boom ground signature. Low-boom aircraft will require precise control of the CG location using a system to automatically distribute the fuel load to achieve a desired CG location. Fuel tank sizes and locations are not available without a detailed structural layout. This can lead to some uncertainty in the CG analysis. Mitigation of this uncertainty could be achieved with wing and fuselage weight estimation using finite-element analysis (FEA) (see Subsection II.D). At this conceptual level, the fuel volume is assumed to be the sum of fixed fractions of the longitudinal wing and fuselage volume distributions. This allows defining a preliminary CG location vs weight diagram when combined with the component weight and CG estimates from FLOPS [52,57].

Landing weight is 70% of MTOGW. The leading and trailing edge flaps are defined by their span ranges for widths and percentages of the wing chords for lengths, which are used by AERO2S [54] for LTO aerodynamics. In this paper, the input parameters for the flaps are fixed. That is, the widths of the flaps are fixed, and the lengths of the flaps change proportionally with the wing chord lengths. Main gear location and length are used in LTO analysis to limit the maximum angle of attack used by the aircraft for LTO to avoid tailstrike. Trimmed aerodynamic polars are generated using AERO2S for three degree-of-freedom LTO calculations by FLOPS [52,53]. For LTO field lengths, insofar as possible with the available data, all relevant FAR Part 25 requirements are met [53]. The stall speeds used in LTO are rough estimates based on the maximum lift coefficient from low-fidelity aero analysis because a high-fidelity Navier-Stokes estimate is prohibitive at the conceptual level where many LTO analyses are required for different flap deflection angles. The basic FAR Part 25 airworthiness requirements are enforced with the estimated stall speeds in LTO analyses.

The center of aerodynamic pressure at the start of cruise for the overland mission is generated using WINGDES [54]. A three-iteration loop is used to adjust the angle of attack so that the total lift from the wing and tail matches the

8

American Institute of Aeronautics and Astronautics

cruise weight. Cruise trim margin and cruise SM are based on the WINGDES center of pressure and the most aft center of gravity for cruise weight.

The LTO and low-boom cruise analysis results will be used to define the involved mission constraints for the low-boom MDO problem formulated in Subsection II.E.

The inputs for calculation of low-boom metrics include the design vector D, weight at the start of cruise, cruise conditions, and baseline $A_{e,r}$ target denoted by $A_{e,r,0}^{target}$ in the previous subsection. The baseline $A_{e,r}$ target is fixed until the baseline geometry is updated by some optimized geometry, which might lead to an updated baseline $A_{e,r}$ target. The baseline $A_{e,r}$ target is scaled using the cruise weights for the current configuration and baseline (see Eq. (2)). The scaled target is propagated through the standard atmosphere to get its sonic boom ground signature using a sonic boom propagation code for solving the augmented Burgers equations [58]. The PLdB value for the ground signature is calculated using the method in Ref. [59].

An aerodynamic analysis code LTSTAR [60] is used to compute A_e due to lift and a modified version of the Harris far-field wave drag program [56] is used for calculation of A_e due to volume. A three-iteration loop is used for LTSTAR to find the required angle of attack so that the total lift from the wing and tail matches the cruise weight. The scaled $A_{e,r}$ target and $A_{e,LoFi}$ are used to compute the A_e matching error $f(D)$ in Eq. (4) or (5).

All key inputs relevant to the low-boom MDO problem in Subsection II.E are included in the green and cyan oval shapes in Fig. 5. The requirements for the low-boom MDO problem will be given in Subsection II.E. The sequential dependencies among the analyses are represented by connecting arrows in Fig. 5.

The MDO architecture in Fig. 5 does not readily fit into one of the existing MDO architectures [44] because NPSS and FLOPS have their own built-in approximation models, optimization algorithms, and disciplinary coupling methods. In this paper, NPSS and FLOPS are used as if they are disciplinary analysis codes. The coupled weight and mission analysis does not change the MDO architecture, but it eliminates two MDO constraints for the range requirements and one MDO input of MTOGW for the low-boom MDO problem in Subsection II.E. The cost is a few iterations between the weight estimation and fixed-range mission analysis, which is far less expensive than the iteration cost for a genetic optimizer in an MDF architecture to find the optimum input MTOGW that satisfies the two range constraints.

D. Calibration of Empirical Aircraft Weights by FEA-based Weight Estimates

The aircraft weights estimation is critical for the low-boom design process, because the weights and CGs determine the takeoff/cruise/landing analyses. To make the low-fidelity multidisciplinary analyses more reliable, an FEA-based weights estimation method [61] is used to calibrate the aircraft weights estimation [57] in FLOPS [52] so that the calibrated FLOPS aircraft weights estimation is an accurate approximation of the FEA-based weights estimation. Figure 6 is a flowchart about how the estimated wing/fuselage weights and MTOGW are updated in the calibration process.
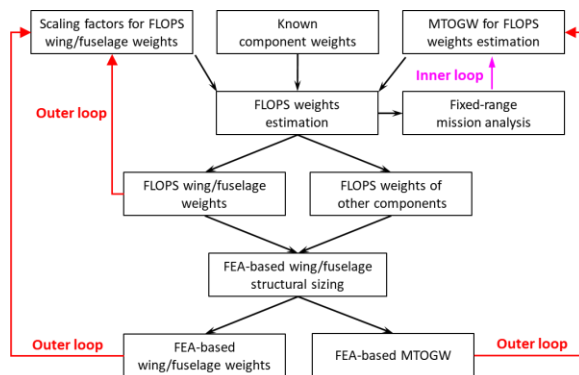

Fig. 6 Calibration of FLOPS weights estimation by FEA-based weights estimation.

The goal of this calibration process is to find the wing and fuselage weight scaling factors used in the FLOPS weights estimation such that the FLOPS wing and fuselage weights are approximately equal to the FEA-based wing and fuselage weights, respectively, for a baseline configuration.

The pink arrow in Fig. 6 completes the inner iteration loop for a converged MTOGW between the FLOPS weights estimation and fixed-range mission analysis. The red arrows in Fig. 6 complete the outer iteration loop for a converged MTOGW between the FLOPS weights estimation and FEA-based weights estimation. The outer iteration loop also finds the calibrated weight scaling factors for wing and fuselage that make the FLOPS wing and fuselage weights equal the FEA-based wing and fuselage weights. Here are the updating formulas for the outer loop in Fig. 6.

9

American Institute of Aeronautics and Astronautics

$$\frac{W_{\text{fuse,fea}}}{W_{\text{fuse,flops}}} \cdot \omega_{\text{fuse}} \mapsto \omega_{\text{fuse}} \tag{6}$$

$$\frac{W_{\text{wing,fea}}}{W_{\text{wing,flops}}} \cdot \omega_{\text{wing}} \mapsto \omega_{\text{wing}} \tag{7}$$

$$\text{MTOGW}_{\text{fea}} = \text{MTOGW}_{\text{flops}} - \left(W_{\text{wing,flops}} - W_{\text{wing,fea}} + W_{\text{fuse,flops}} - W_{\text{fuse,fea}}\right) \tag{8}$$

$\text{MTOGW}_{\text{fea}}$ given in Eq. (8) is used as the initial guess for MTOGW in the inner iteration loop for the coupled weight and mission analysis. The iteration process terminates when the FLOPS wing and fuselage weights are approximately equal to the FEA-based wing and fuselage weights, respectively.

If the iteration process terminates successfully, then the mission analysis, FLOPS weights estimation, and FEA-based weights estimation are performed using the same MTOGW. Moreover, the FEA-based weights estimation and FLOPS have the same estimates for wing and fuselage weights.

For the FLOPS weights estimation used in this paper, the FEA-based calibration factors ω_{fuse} and ω_{wing} are 0.8 and 1, respectively. The calibrated weight scaling factors were generated using a vision concept for low-boom supersonic transports and are fixed for all the FLOPS fuselage and wing weight estimates in this paper. The load conditions for FEA-based structural sizing were based on pull-up, cruise, and push-over maneuvers at the start of cruise. Three FEA models and sizing examples for supersonic configurations using the same FEA-based weight estimation method are included in Ref. [61].

E. Low-Boom MDO Problem with Mission Constraints

With the MDF architecture in Fig. 5, the low-boom MDO problem for conceptual inverse design of low-boom supersonic aircraft with mission constraints can be written as a standard multiobjective optimization problem.

$$\min_{\boldsymbol{D}} \{f(\boldsymbol{D}), \text{MTOGW}\} \text{ subject to } g_i(\boldsymbol{D}) \geq 0 \text{ for } 1 \leq i \leq 7 \text{ and } \boldsymbol{l} \leq \boldsymbol{D} \leq \boldsymbol{u} \tag{9}$$

The design vector $\boldsymbol{D}$ is the collection of 42 design variables described in Subsection II.A: 11 fuselage parameters, 24 wing and tail parameters, engine thrust, and 6 auxiliary LTO parameters. The objective function $f(\boldsymbol{D})$ is the A_e matching error defined in Eq. (4) or (5).

The mission requirements are based on an unpublished ongoing economic feasibility study for supersonic transports and subject to change. Under some preliminary economic assumptions, a low-boom supersonic configuration would be economically viable if it could carry 40 passengers, fly an overwater mission with cruise Mach of 1.8 and range of at least 3,200 nm (which will be changed to 3,600 nm later), and fly a low-boom overland mission with cruise Mach of 1.6 and range of at least 2,500 nm. The requirement for 40 passengers is enforced with fuselage volume constraints and payload weight. Fuselage volume constraints for 40 passenger seats and main gear storage are implemented using the lower bounds for the fuselage width design variables. The maximum cruise Mach 1.8 for the overwater mission is based on LTO noise, emissions, and technology availability for an advance engine model. The minimum range requirements are based on the origin-destination pairs in the continent US and transatlantic commercial flights. The MDF architecture in Fig. 5 eliminates two constraints for two range requirements and changes MTOGW to an output of the fixed-range dual-mission analysis. The cruise altitudes for the dual mission are design variables, but they are fixed for the low-boom MDO in this paper. Their fixed values are chosen based on the following trade rules between performance and low-boom benefits. For a given low-boom vehicle, lower cruise altitudes result in lower ground noise levels but reduced performance. So, the cruise altitude for the overland mission is fixed at 45,000 ft for the maximum low-boom benefit while avoiding the cruise altitude range for subsonic transports. The cruise altitude for the overwater mission is limited to 60,000 ft for maximum performance benefit allowed by the engine.

The constraints $g_i(\boldsymbol{D}) \geq 0$ ($1 \leq i \leq 7$) in Eq. (9) correspond to the following mission constraints.

(II.E.1)   Trim margin for overland cruise ≥ 1 ft (*i.e.*, with fuel redistributions, the longitudinal CG can be placed at least 1 ft behind the center of aerodynamic pressure at the start of cruise for the overland mission)

(II.E.2)   CG margin to prevent tip over on the ground ≥ 4 ft (*i.e.*, the longitudinal CG of the aircraft at empty weight is at least 4 ft before the main gear longitudinal location)

(II.E.3)   Cruise static margin for the overland mission $\geq 2\%$

(II.E.4)   LTO margins $\geq 2\%$

(II.E.5)   LTO field lengths $\leq 8,300$ ft

(II.E.6)   Approach velocity ≤ 150 knots

(II.E.7)   Tail rotation angles for trim at LTO ≥ -20°

A more comprehensive conceptual design of low-boom supersonic aircraft might use more constraints, but these constraints include the most significant constraints that could conflict with the low-boom inverse design objective.

The trim constraint for low-boom cruise was discussed in Subsection II.C. Constraint (II.E.2) prevents tip over on the ground when the aircraft is empty. Constraints (II.E.3) and (II.E.4) are typical longitudinal stability constraints for aircraft conceptual design. The constraints on LTO field lengths are determined by the relevant service airports and some margin for potential errors in the FLOPS estimates of LTO field lengths. The maximum approach velocity of 150 knots is used to mitigate the approach noise. Because AERO2S [54] uses linear aerodynamics for LTO trim analyses, the limit of -20° on tail deflections for trim during LTO is used in (II.E.7).

However, a Pareto point for Eq. (9) must satisfy the following two additional constraints to be a *plausible low-boom* design.

$$f(\boldsymbol{D}) \leq 0.015 \cdot A_{e,\mathrm{LoFi}}(l_e, \boldsymbol{D}) \text{ and PLdB for } A_{e,r}^{\mathrm{target}}(\boldsymbol{D}) \leq 70 \qquad (10)$$

The relative error tolerance factor of 0.015 can be replaced with any sensible small number that ensures a visually good match between $A_{e,\mathrm{LoFi}}(x_e)$ and $A_{e,r}^{\mathrm{target}}(x_e)$ for x_e up to the aft part of the wing. The first constraint in Eq. (10) aims to satisfy the near zero matching error requirement of the low-boom inverse design optimization: the low-boom inverse design objective function $f(\boldsymbol{D})$ must be close to zero for the aircraft shape generated by $\boldsymbol{D}$ to have a low-boom front shape. A plausible low-boom design must be further refined by CFD-based low-boom shaping methods to attain a completely shaped low-boom ground signature. The target PLdB limit of 70 is based on the NASA N+3 goal [15,17] for low-boom supersonic transports.

In theory, the mathematical low-boom MDO problem is to minimize MTOGW subject to the mission constraints (II.E.1)-(II.E.7) and two low-boom constraints in Eq. (10). Unfortunately, any of the two low-boom constraints in Eq. (10) will make most designs in any design space infeasible. So, Eq. (10) will only be checked once the Pareto frontier of Eq. (9) is generated. If none of the Pareto points satisfies Eq. (10), it means that Eq. (9) does not have a plausible low-boom solution. In such a case, one has the option of relaxing the design requirements on the overland cruise Mach/range or increasing the aircraft length for a solution of Eq. (9) that also satisfies Eq. (10). The low-boom constraints in Eq. (10) makes the low-boom supersonic concept development extremely difficult.

F. Block Coordinate Optimization Method for Low-Boom MDO

Preliminary trials with a direct optimization solution approach for Eq. (9) did not yield any plausible low-boom design. Existing derivative-free optimization algorithms are neither efficient nor effective to solve a multiobjective optimization problem with 42 design variables and 10 nonlinear constraints. Lack of intuition about the solvability of Eq. (9) with the low-boom constraints in Eq. (10) makes it difficult to determine the design vector bounds l and $\boldsymbol{u}$ that would contain a plausible low-boom design.
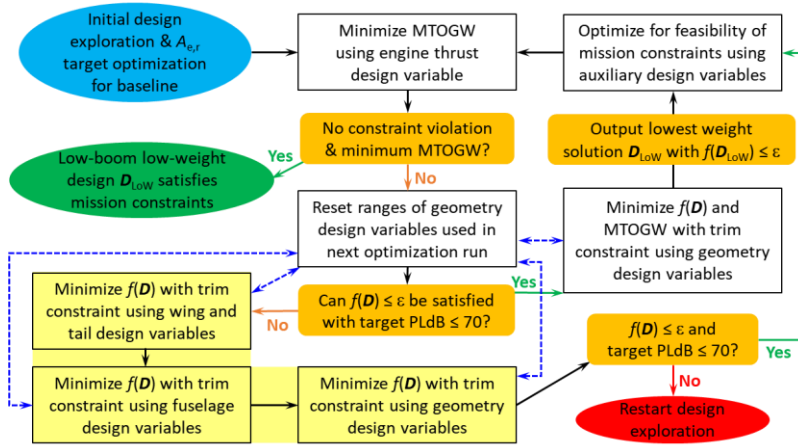

Fig. 7 BCO for low-boom MDO.

A careful examination of the low-boom design problem reveals that Eq. (9) can be partitioned into the following simpler subproblems: (i) use design exploration to find a good baseline configuration (such as minimizing MTOGW

American Institute of Aeronautics and Astronautics

of the baseline using engine thrust etc.); (ii) use 24 wing/tail design variables to tailor the lift distribution and reduce the low-boom objective defined by Eq. (4) with the trim constraint; (iii) use 11 fuselage design variables to minimize the low-boom objective defined by Eq. (5) with the trim constraint; (iv) repeat Steps (ii) and (iii) until the optimal solution satisfies Eq. (10), with the options of using all geometry design variables simultaneously and/or minimizing the low-boom objective and MTOGW simultaneously; (v) use 6 auxiliary LTO design variables to satisfy the specified mission constraints; (vi) minimize MTOGW with respect to the engine thrust; and (vii) repeat the previous steps if Eq. (10) is not satisfied, or MTOGW can be reduced further, or there is any mission constraint violation. These steps can be represented by the flowchart in Fig. 7.

BCO in Fig. 7 can be considered as a variation of the block coordinate descent method (see, *e.g.*, Ref. [62]). Here the design vector D is partitioned into 4 blocks (subsectors) during the initial phase of minimizing $f(D)$: (i) engine thrust, (ii) wing and tail design variables, (iii) fuselage design variables, and (iv) auxiliary LTO design variables. Numerical optimization is performed for each block of design variables successively. In theory, the design space $l \leq D \leq u$ should include all reasonable supersonic configurations and be fixed for all optimization runs. In practice, only very limited ranges for the geometry design variables can be used for an effective and efficient solution of minimizing $f(D)$ with the trim constraint. So, Fig. 7 includes an unconventional step for numerical optimization – the modifications of geometry design variable ranges for the current BCO iteration involving minimization of $f(D)$. This unconventional step in Fig. 7 is represented by a box to reset the ranges of the design variables for optimization, which is a common engineering practice for solving real-world optimization problems. The blue link represents the optional path for the current BCO iteration using a different set of geometry design variable ranges. The blue link is only used if an optimized geometry design variable is close to one of its bounds, which indicates that the optimized design variable might not be fully optimized due to a restrictive range for computational effectiveness and efficiency of a genetic optimizer. The general rule is to reset the design variable range such that the optimized design variable is near the mid location of the design range. This will ensure that the optimized design variables represent a local optimal solution from the genetic optimizer (if it converges). The termination of each optimization run is mainly determined by how much time could be spent before knowing whether the next optimal solution is useful or not.

If no plausible low-boom solution satisfying Eq. (10) could be found (which is not uncommon), it means a restart of the low-boom concept development process. The restart usually involves design requirement changes, design variable changes, and/or aircraft length change. The aircraft length change might lead to very time-consuming design layout changes with reconsideration of component locations, main gear longitudinal location, passenger cabin, and fuselage volume constraints for passengers and main gear storage.

After a plausible low-boom design satisfying Eq. (10) is found, the highlighted yellow boxes in Fig. 7 will not be executed anymore. The design vector D is repartitioned into 3 blocks: (i) engine thrust, (ii) all geometry design variables, and (iii) auxiliary LTO design variables. The design goal is to find the lowest weight solution on the Pareto frontier of Eq. (9) that also satisfies Eq. (10). The BCO iteration in Fig. 7 is terminated when MTOGW cannot be significantly reduced by the engine thrust optimization for a plausible low-boom design.

A block coordinate descent method does not include any constraint or design variable range modifications. It does not require an optimal solution for a given block of coordinates; instead, only a sufficient reduction of the objective function is required for each block coordinate descent iteration. Its convergence was proved for a nonconvex and nondifferentiable objective function under some separation assumptions for block coordinates [62]. The proposed BCO method solves an optimization problem for each block of design variables and uses partitions of the objectives and constraints for a constrained multiobjective optimization problem. The transition between two BCO iterations is performed manually and might involve the design variable range modifications (except some lower bounds for fuselage widths) when any of geometry design variable is too close to its lower or upper bound. This method aims to overcome the ineffectiveness and inefficiency of a genetic optimizer to generate the Pareto frontier of a constrained multiobjective optimization problem with potentially undefined values for the objective and constraint functions. It is a special numerical optimization method using an MDF architecture. No proof of its convergence is available. The successful application of this method in Section III for finding a Pareto point of Eq. (9) that also satisfies Eq. (10) demonstrates its validity.

A theoretical rationale for a partition between fuselage and wing/tail design variables is the following. Suppose that an ideal optimal solution exists with the A_e matching error = 0. Then

$$A_{e,\text{LoFi}}^{\text{lift}}(x_e) + A_e^{\text{volume}}(x_e) = A_{e,\text{LoFi}}(x_e) = A_{e,r}^{\text{target}}(x_e) \quad \text{for } 0 \leq x_e \leq \lambda \tag{11}$$

If both the wing and fuselage design variables are used to reduce the A_e matching error, an optimizer might not know that it is more desirable to use the lift distribution than the fuselage width distribution for a reduction of the A_e matching error. The separation of wing/tail lift tailoring and fuselage volume shaping helps minimize unnecessary

American Institute of Aeronautics and Astronautics

fuselage width changes during optimization and avoids a wavy fuselage shape of a low-boom design. The wing/tail lift tailoring focuses on reducing the major trend differences (defined by Eq. (4)) between the $A_{e,r}$ target and $A_{e,LoFi}$ of the design, while the fuselage width shaping aims at reducing the average differences (defined by Eq. (5)) between the $A_{e,r}$ target and $A_{e,LoFi}$ of the design.

III. Numerical Results

BCO in Fig. 7 is successfully applied to find a plausible low-boom design that satisfies the specified mission constraints. The following subsections document how the plausible low-boom design is generated.

A. Baseline Analysis

The baseline geometry is given in Subsection II.A. The engine thrust for the baseline is 49,000 lb. The initial values for the auxiliary LTO design variables are given in Table 1. The initial values for the wing planform and fuselage design variables are given in Figs. 2 and 3. The initial values for the wing camber design variables and five horizontal tail parameters are of secondary importance and not listed here. The following are the constraint values for the baseline.

(III.A.1)   Trim margin for overland cruise = 0.16 ft (infeasible value)
(III.A.2)   CG margin to prevent tip over on the ground = 17.3 ft
(III.A.3)   Cruise static margin for the overland mission = 16.8%
(III.A.4)   Takeoff static margin = 1.5% (infeasible value) and landing static margin = 3.5%
(III.A.5)   LTO field lengths are 6,867 ft and 7,482 ft, respectively
(III.A.6)   Approach velocity = 128 knots
(III.A.7)   Tail rotation angles for trim at LTO are -7.8° and -11.3°, respectively

The $A_{e,LoFi}$ distribution of the baseline differs significantly from its low-boom target over the specified effective distance interval from 0 ft to λ_0 = 194.7 ft (see Fig. 8). The dash vertical line in Fig. 8 shows the location of λ_0 used in Eq. (3) to define the upper limit for A_e matching error calculation.
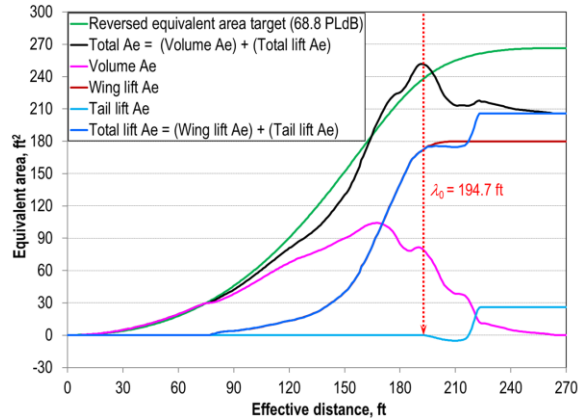
Fig. 8 A_e **distributions for baseline.**

B. Lift Tailoring

Lift tailoring with the 24 wing and horizontal tail design variables is very effective to reduce the maximum A_e matching error while maintaining the trim margin of 1 ft for overland cruise. Initially, when the design variable ranges are large and/or there is no knowledge about how to avoid mission analysis failures with appropriate bounds on the design variables, the Non-Dominant Sorting Genetic Algorithm II in ModelCenter [63] is used for optimization. Later, when relatively small ranges for the design variables are used and mission analysis failures become rare, the Design Explorer (a derivative-free optimization code using surrogate models for gradient-based optimization iterations) in ModelCenter is used for optimization. Between two successive lift tailoring optimization runs (following the blue arrow connecting the block for minimizing $f(\mathbf{D})$ using the wing and tail design variables in Fig. 7), the optimal solution of the first optimization run is used as the initial design for the next optimization run and the ranges of the design variables are updated to set each initial design variable near the mid location of the design range if possible. The final optimization solution is obtained using the Design Explorer (for efficiency). The A_e distributions of the lift tailoring optimization solution are shown in Fig. 9. The wing shape changes are illustrated in Fig. 10. Note that the z-axis is

magnified 5 times to provide a better view for airfoil changes. The most visible changes are a reduction of the wingspan from 98 ft to 92 ft and more aft position of the tip airfoil.
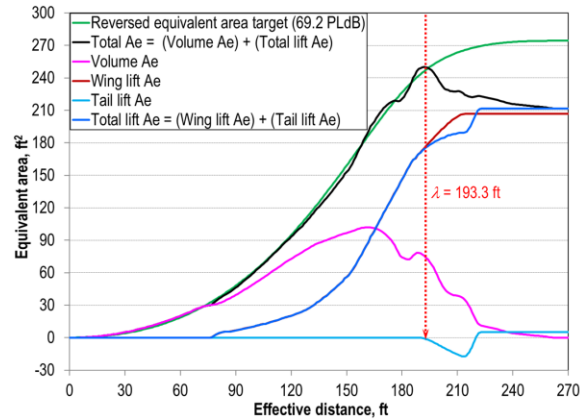

Fig. 9 A_e **distributions for lift tailoring solution.**

a) Wing planforms
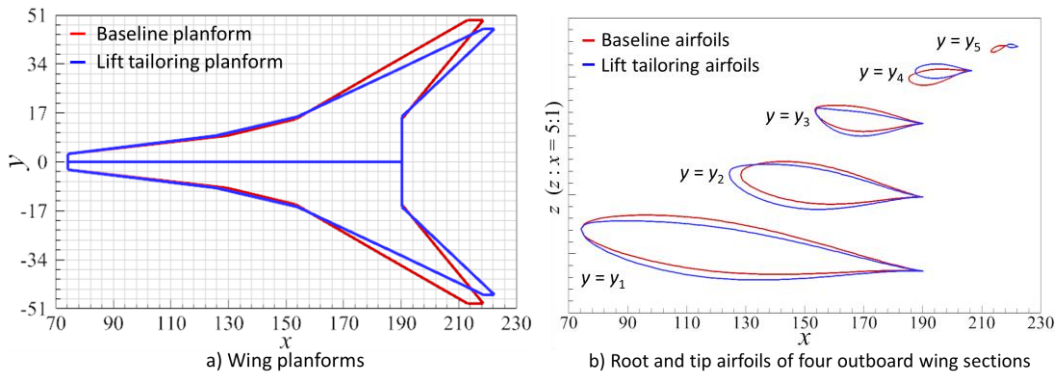
b) Root and tip airfoils of four outboard wing sections

Fig. 10 Wing shapes of baseline and lift tailoring solution.

C. Fuselage Volume Shaping

The low-boom objective $f(\mathbf{D})$ defined by Eq. (5) can be further reduced by fuselage volume shaping. The fuselage volume shaping problem is relatively easy to solve because the fuselage width changes rarely cause a mission analysis failure. The A_e distributions and difference $(A_{e,r}^{target} - A_{e,LoFi})$ are plotted in Fig. 11. The final optimization solution is obtained using the Design Explorer. The fuselage width comparison is shown in Fig. 12.

a) Equivalent areas for fuselage volume shaping solution

b) A_e matching improvement by volume shaping
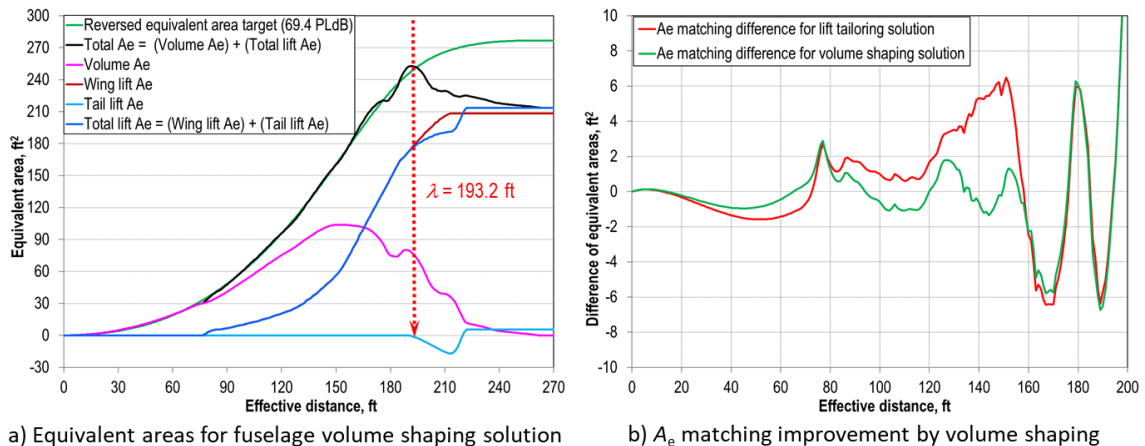
Fig. 11 Reduction of A_e matching error by fuselage volume shaping solution.

14

American Institute of Aeronautics and Astronautics
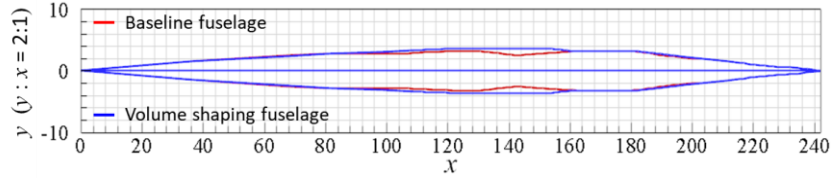
Fig. 12 Fuselage width distributions of baseline and volume shaping solution.

D. Low-Boom Optimization

Finally, the low-boom inverse design optimization is performed for all geometry design variables with relatively small ranges for the design variables to reduce the low-boom design objective defined by Eq. (5). In this case, the number of design variables is so large that ModelCenter's Design Explorer cannot be used as a solver. The Non-Dominant Sorting Genetic Algorithm II in ModelCenter is used to find the optimal solution of the low-boom optimization problem with 35 shape design variables and the trim constraint. After 77 hours of wall-clock time (using a mix of desktop computers, Windows servers, and Linux servers), the genetic optimization algorithm terminates when reaching the maximum number (10,000) of design evaluations.

Table 2 Geometry design variables and their bounds for low-boom optimization solution

Wing camber	$0 \le \delta_{1,max} = 0.0004 \le 0.1$	$0 \le \delta_{2,max} = 0.004 \le 0.25$	$0 \le \delta_{3,max} = 0.132 \le 0.2$
	$0 \le \delta_{4,max} = 0.03 \le 0.2$	$0 \le \tau_{1,max} = 0.06 \le 0.2$	$0 \le \tau_{2,max} = 0.11 \le 0.25$
	$0 \le \tau_{3,max} = 0.22 \le 0.25$	$0 \le \tau_{4,max} = 0.0 \le 0.2$	$-5 \le \theta_4 = -1.7 \le -1$
	$-2 \le \theta_5 = 1.1 \le 2$		
Wing planform	$6 \le s_2 = 6.5 \le 7$	$5.9 \le s_3 = 6.5 \le 6.6$	$14.5 \le s_4 = 15.8 \le 17$
	$13 \le s_5 = 14.7 \le 15.6$	$115.4 \le c_1 = 116.3 \le 116.8$	$61.9 \le c_2 = 64.9 \le 66.9$
	$36.2 \le c_3 = 36.6 \le 38.2$	$3.4 \le c_5 = 4.2 \le 5.7$	$219 \le x_{tip} = 219.1 \le 224$
Horizontal tail	$16 \le span = 18.1 \le 19$	$47 \le sweep = 50.4 \le 52$	$27 \le c_{root} = 28.8 \le 31$
	$4 \le c_{tip} = 9.3 \le 11$	$-4 \le \theta_{htail} = -3.3 \le 0$	
Fuselage width	$65.3 \le x_1 = 68.2 \le 70.1$	$101.6 \le x_2 = 108.1 \le 113.7$	$118.6 \le x_3 = 124.5 \le 128.3$
	$147.6 \le x_4 = 154.1 \le 157.3$	$4.5 \le d_1 = 4.85 \le 5.5$	$5.4 \le d_2 = 6.78 \le 7.2$
	$5.58 \le d_3 = 7.25 \le 7.44$	$5 \le d_4 = 7.50 \le 8.5$	$6.3 \le d_5 = 6.30 \le 7.6$
	$6.3 \le d_6 = 6.75 \le 7.6$	$4.5 \le d_7 = 5.15 \le 5.5$	

The ranges and values of the design variables for the low-boom optimization solution are listed in Table 2. Recall that the design variable bounds are not known *a priori* and determined by successive optimization runs with empirical adjustments of the bounds. The basic rule is that the optimal design variable should not attain any specified upper or lower bound if the bound is not determined by the volume constraints for passengers and main gear storage.
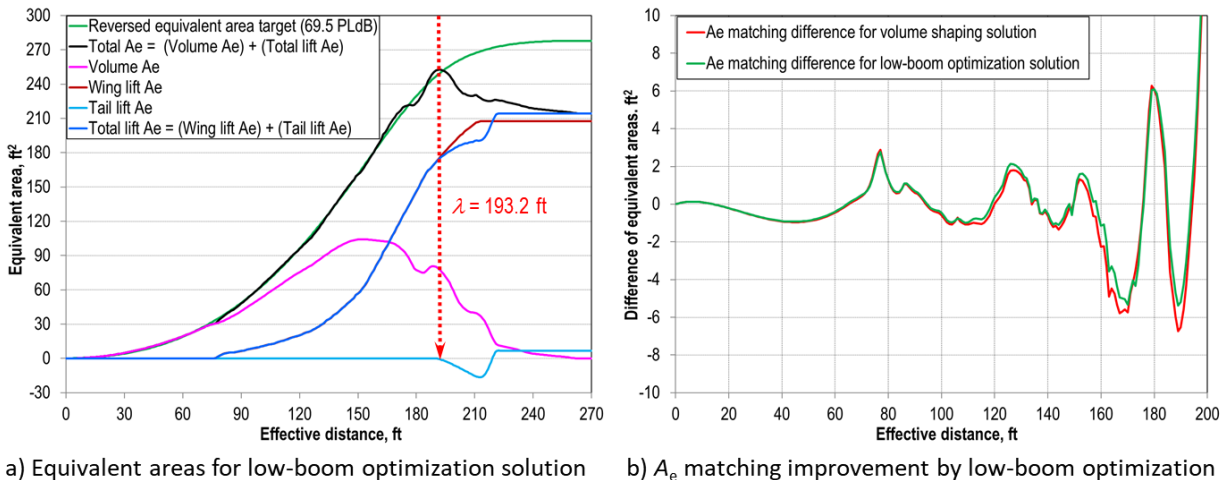
a) Equivalent areas for low-boom optimization solution   b) A_e matching improvement by low-boom optimization

Fig. 13 Reduction of A_e matching error by low-boom optimization solution.

15

American Institute of Aeronautics and Astronautics

Figure 13 shows the A_e distributions and difference ($A_{e,r}^{target} - A_{e,LoFi}$) for the low-boom optimization solution. Only marginal matching error reduction is achieved as shown in Fig. 13 b). This indicates that the separation of lift tailoring and volume shaping does not lead to a severe penalty for minimizing the low-boom objective with the trim constraint. The lower width bounds for the cabin defined in Eq. (1) are relaxed for a better reduction of the A_e matching error. But the optimal width parameters are large enough to maintain enough fuselage volume for 40 passenger seats and main gear storage.

E. Feasibility Optimization

The low-boom optimization solution satisfies Eq. (10), so the next block of auxiliary LTO design variables is optimized to satisfy the mission constraints (see the right green arrow in Fig. 7). The six auxiliary design variables have almost no effect on the A_e matching error. The bounds of the design variables and values for the feasibility optimization solution are listed in Table 3. The objective function is the least square sum of the deflection angles and CG offsets.

Table 3 Auxiliary LTO design variables and their bounds for feasibility optimization solution

$0 \le$ TE flap deflection angle for takeoff $= 5.7 \le 16$	$10.5 \le$ Main gear length $= 10.7 \le 11.4$
$0 \ge$ LE flap deflection angle for landing $= -0.1 \ge -2$	$0 \le$ Longitudinal CG offset for takeoff $= 9.5 \le 11$
$0 \le$ TE flap deflection angle for landing $= 7.0 \le 13$	$0 \le$ Longitudinal CG offset for landing $= 9.1 \le 11$

The following are the feasible constraint values for the feasibility optimization solution.
- (III.E.1) Trim margin for overland cruise = 1.0 ft
- (III.E.2) CG margin to prevent tip over on the ground = 17.5 ft
- (III.E.3) Cruise static margin for the overland mission = 16.4%
- (III.E.4) LTO static margins are 2.0%
- (III.E.5) LTO field lengths are 7,995 ft and 7,820 ft, respectively
- (III.E.6) Approach velocity = 143 knots
- (III.E.7) Tail rotation angles for trim at LTO are -8.9° and -11.6°, respectively

F. Engine Thrust Optimization

The previously optimized engine thrust for the baseline might not be optimal anymore. So, the MTOGW of the feasibility optimization solution is minimized again with respect to the engine thrust. The optimal engine thrust is 47,950 lb. The minor change of the engine thrust has a negligible effect on the low-boom characteristics; the two low-boom designs for engine thrusts of 49,000 lb and 47,950 lb have nearly identical A_e distributions (see Fig. 14).

a) $A_{e,r}$ targets and A_e distributions
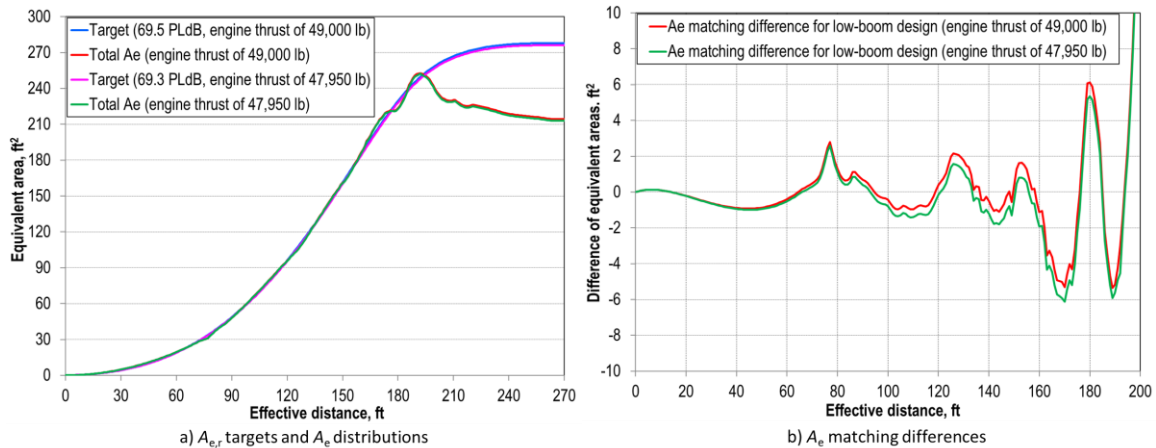
b) A_e matching differences

Fig. 14 Comparison of low-boom solutions for engine thrusts of 49,000 lb and 47,950 lb.

The low-boom design for engine thrust of 47,950 lb also satisfies the specified mission constraints.
- (III.F.1) Trim margin for overland cruise = 1.05 ft
- (III.F.2) CG margin to prevent tip over on the ground = 17.5 ft
- (III.F.3) Cruise static margin for the overland mission = 16.5%

American Institute of Aeronautics and Astronautics

(III.F.4)   Takeoff static margin = 2.1% and landing static margin = 2.0%
(III.F.5)   Takeoff field length = 7,897 ft and landing field length = 7,962 ft
(III.F.6)   Approach velocity = 143 knots
(III.F.7)   Tail rotation angle for trim at takeoff = -11.5° and tail rotation angle for trim at landing = -9.0°

Table 4 gives a weight comparison of these two low-boom designs. The weight differences are negligible. The engine thrust optimization does not significantly change the optimality of the specified engine thrust of 49,000 lb determined by a parametric study of the engine thrust for the baseline.

Table 4 Weight comparison of two low-boom designs

	Low-boom MTOGW	Overwater MTOGW	Zero-fuel weight
Low-boom design for engine thrust of 49,000 lb	200,493 lb	192,756 lb	100,694 lb
Low-boom design for engine thrust of 47,950 lb	199,334 lb	193,240 lb	100,543 lb

This terminates the BCO iteration for finding a plausible low-boom design satisfying Eq. (10) (see Fig. 7). The BCO method enters the 2nd phase of finding the lowest weight solution of Eq. (9) that also satisfies Eq. (10).
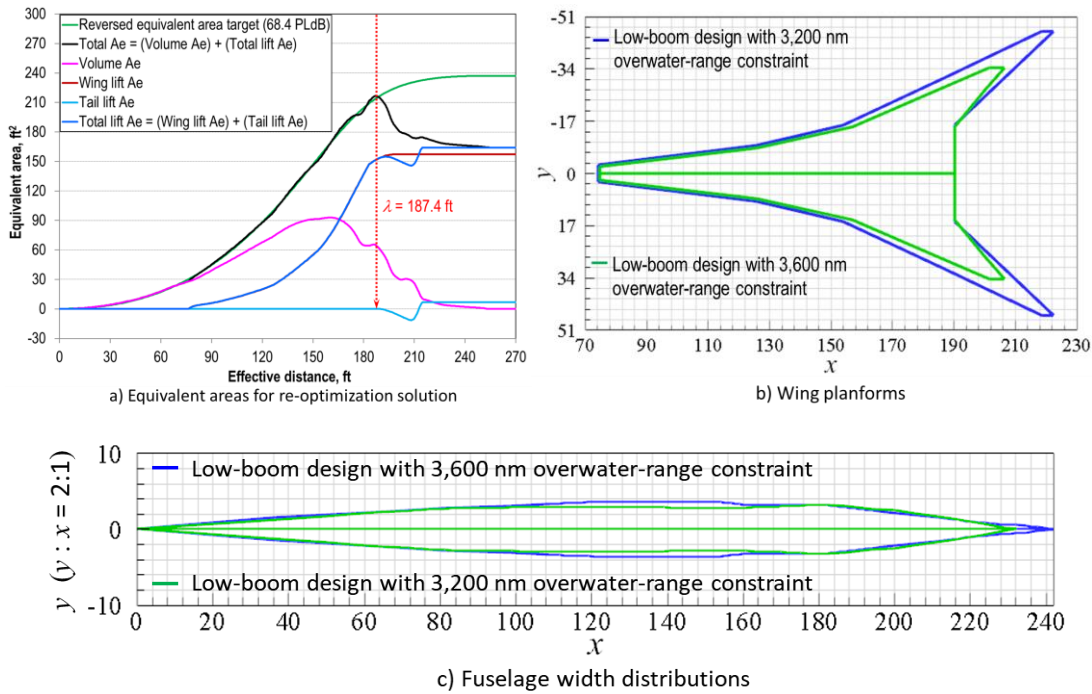
Fig. 15 A_e **distributions and shape changes for re-optimization solution.**

G. Re-optimization for Requirement Change

Unfortunately, for aircraft conceptual design, it often happens that some critical assumptions for the design problem were found to be incorrect after the design problem had been solved successfully. An updated economic feasibility study of the previously generated plausible low-boom supersonic concept shows that winds have a significant effect on transatlantic flights and an overwater mission range of 3,600 nm for FLOPS is a more realistic requirement. The previous low-boom configuration with engine thrust of 47,950 lb can carry an additional 6,093 lb of fuel on the overwater mission to then match the low-boom MTOGW (see Table 4) and increase its overwater range to 3,402 nm; but this does not meet the new requirement for overwater range of 3,600 nm. So, the configuration is redesigned with the 3,600 nm overwater-range constraint. To improve aerodynamic performance, the wingspan is constrained to be as short as possible. After applying BCO with simultaneous minimization of $f(D)$ and MTOGW, the final design is a much lighter low-boom supersonic aircraft (with MTOGW = 157,583 lb) that flies 3,600 nm (instead of 3,200 nm) overwater at cruise Mach 1.8. The corresponding low-boom target has an undertrack ground noise level of 67.8 PLdB. The lower noise level of 67.8 PLdB shows that there is some excess margin for the low-

17

American Institute of Aeronautics and Astronautics

boom target and a shorter vehicle might still be able to satisfy the low-boom constraints in Eq. (10). So, a re-optimization iteration begins to shorten the aircraft length to 232 ft. Such design iterations for changing assumptions and requirements are typical for low-boom aircraft conceptual design. BCO is applied again to generate a re-optimization solution of Eq. (9). The re-optimization solution satisfies all the specified mission constraints and Eq. (10). It also has a lower MTOGW than the previous low-boom design with fuselage length of 242 ft. Figure 15 a) shows the A_e distributions of the re-optimization solution. Figures 15 b) and c) compare the wing planforms and fuselage width distributions, respectively, of the two low-boom designs with two different overwater-range constraints. The fuselage width distribution of the re-optimization solution has a minimum width of 5.5 ft, but it still has enough volume for 40 passengers and main gear storage (see Fig. 16, where the pilots and passengers are imported from an Uber eVTOL common reference model [64]).
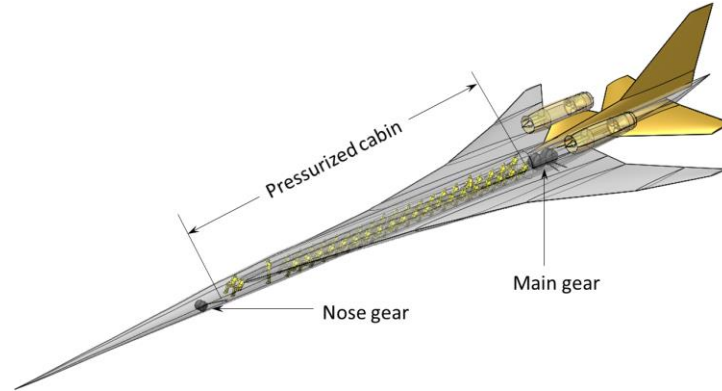
Fig. 16 Cabin arrangement and main gear packaging for re-optimization solution.

The mission constraint values for the re-optimization solution are feasible.
(III.G.1)   Trim margin for overland cruise = 3.69 ft
(III.G.2)   CG margin to prevent tip over on the ground = 13.1 ft
(III.G.3)   Cruise static margin for the overland mission = 18.0%
(III.G.4)   LTO static margins are 2.0% and 2.1%, respectively
(III.G.5)   LTO field lengths are 8,003 ft and 8,280 ft, respectively
(III.G.6)   Approach velocity = 150 knots
(III.G.7)   Tail rotation angle for trim at LTO are -6.0° and -6.6°, respectively

Table 5 compares some specifications of the two low-boom designs with two different overwater-range constraints. It is obvious *now* that the low-boom design with the 3,200 nm overwater-range constraint would have a much lower MTOGW if the wingspan were constrained properly and simultaneous minimization of the low-boom objective and MTOGW were performed. Note that the wingspan of 98 ft of the baseline (see Fig. 3) was based on previous design exploration results; the BCO iterations in the previous subsections searched for an optimal low-boom solution with the specified mission constraints in a design space around the baseline, which did not include configurations with spans as short as 69 ft. Applications of knowledge gained during successive BCO runs eventually lead to a much lighter low-boom design for the overwater range of 3,600 nm. The MTOGW reduction is mainly due to the reductions of wingspan, engine thrust, and fuselage length. A further reduction of the engine thrust could lead to a lower MTOGW, but it would require a maximum takeoff field length more than 8,300 ft.

The re-optimization process is terminated by the constraint for maximum takeoff field length of 8,300 ft. A further reduction of the fuselage length is not possible because of the cabin length and component layout restrictions, unless the longitudinal seat spacing of 4 ft is reduced. So, this low-boom concept is considered to be optimal for the specified longitudinal seat spacing of 4 ft, maximum LTO field length of 8,300 ft, low-boom cruise Mach 1.6 for a range of 2,500 nm at cruise altitude of 45,000 ft, overwater cruise Mach 1.8 for a range of 3,600 nm at optimum cruise altitude with a ceiling of 60,000 ft, and low-boom constraints in Eq. (10). Any change of these requirements/assumptions could potentially lead to significant changes of the resulting low-boom concept.

Table 5 Comparison of two low-boom designs with two different overwater-range constraints

	Overwater range of 3,200 nm	Overwater range of 3,600 nm
Engine thrust	47,950 lb	36,700 lb
Fuselage length	242 ft	232 ft

American Institute of Aeronautics and Astronautics

Wingspan	92 ft	69 ft
Wing area	3,678 ft^2	3,009 ft^2
Zero-fuel weight	100,543 lb	76,249 lb
Low-boom MTOGW	199,334 lb	154,474 lb
Overwater MTOGW	193,240 lb	153,212 lb

IV. Concluding Remarks

The block coordinate optimization (BCO) method for the low-boom MDO problem with the specified mission constraints is successfully applied to generate a low-boom supersonic transport for 40 passengers at a cruise Mach of 1.6 with a range of 2,500 nm. The generated low-boom configuration can also perform an overwater mission at cruise Mach 1.8 for a range of 3,600 nm. The remaining mission constraints including the trim constraint for low-boom cruise and static margins for takeoff/cruise/landing are also satisfied. A total of 42 design variables are used for MDO, including the engine thrust, fuselage cross section widths and locations, wing and horizontal tail shape parameters, and six auxiliary control parameters for LTO. The volume constraints for 40 passengers and main gear storage are enforced by the lower bounds on the fuselage width design variables. The most difficult challenge is to resolve the conflict between attaining a desirable low-boom design objective and maintaining the aircraft longitudinal CG ahead of the aerodynamic center of pressure at the start of cruise of the overland mission. The latter constraint is referred to as the trim constraint. The low-boom inverse design objective and trim constraint are both mainly determined by the volume and lift distributions of the configuration. Finding the best compromise between them is a difficult optimization problem, which might only have an optimum solution with a relatively high equivalent area matching error and does not lead to a plausible low-boom design. Furthermore, potential mission analysis failures due to insufficient thrust and/or poor aerodynamic performance make the objective and constraint functions of the low-boom MDO problem undefined for some points in the design space, effectively forcing the use of genetic optimization algorithms for an optimal solution. Even if there exists a feasible solution for the low-boom MDO problem with the specified mission constraints, it is difficult to know *a priori* what design variables and their ranges are sufficient to obtain such a solution. The successful application of BCO shows that such a difficult MDO problem is solvable.

It is well known that low-fidelity aerodynamics and CFD yield different lift distributions for a supersonic configuration. A natural question is whether the feasibility of a low-fidelity low-boom MDO problem can be retained using high-fidelity analyses. A theoretical hypothesis with empirical evidence is provided in Section I to justify why matching the low-fidelity equivalent area distribution to a reversed equivalent area target could lead to a CFD-based low-boom design satisfying the same mission constraints. Moreover, the calibration of empirical aircraft weights estimation by FEA-based wing and fuselage weight estimates in Subsection II.D shows that the weights and CGs could be calculated using a multifidelity approach so that they are consistent with FEA-based analysis results. The consistency between low-fidelity and high-fidelity aerodynamic performance analyses will be studied in the future.

In conclusion, the proposed BCO method is calibrated with CFD and FEA analyses for its reversed equivalent area target and fuselage/wing weights. It has been used to generate a plausible low-boom configuration that satisfies all the specified mission constraints and has a low-boom front shape matching a low-boom reversed equivalent area target with a ground noise level below 70 PLdB. The next step is to demonstrate that the existence of such a low-fidelity low-boom design implies the feasibility of a CFD/FEA-based low-boom design for the same mission constraints.

Acknowledgments

References

[1] Farhat, C., Maute, K., Argrow, B., and Nikbay, M., "Shape Optimization Methodology for Reducing the Sonic Boom Initial Pressure Rise," *AIAA Journal*, Vol. 45, No. 5, 2007, pp. 1007–1018. doi:10.2514/1.27607

[2] Li, W., Campbell, R., Geiselhart, K., Shields, W., Nayani, S., and Shenoy, R., "Integration of Engine, Plume, and CFD Analyses in Conceptual Design of Low-Boom Supersonic Aircraft," AIAA Paper 2009-1171, June 2009. doi:10.2514/6.2009-1171

[3] Ordaz, I., and Li, W., "Integration of Off-Track Sonic Boom Analysis in Conceptual Design of Supersonic Aircraft," AIAA Paper 2011-464, June 2011. *Journal of Aircraft*, Vol. 51, No. 1, 2014, pp. 23–28. doi:10.2514/6.2011-464

[4] Ordaz, I., Li, W., and Campbell, R., "Automated Tetrahedral Mesh Generation for CFD Analysis of Aircraft in Conceptual Design," AIAA Paper 2014-0118, June 2014. doi:10.2514/6.2014-0118

[5]   Park, M., and Nemec, M., "Nearfield Summary and Statistical Analysis of the Second AIAA Sonic Boom Prediction Workshop," AIAA Paper 2017-3256, June 2017. *Journal of Aircraft*, Vol. 56, No. 3, 2019, pp. 851-875. doi:10.2514/6.2017-3256

[6]   Li, W., and Rallabhandi, S., "Inverse Design of Low-Boom Supersonic Concepts Using Reversed Equivalent-Area Targets," AIAA Paper 2011-3498, June 2011. *Journal of Aircraft*, Vol. 51, No. 1, 2014, pp. 29–36. doi:10.2514/1.C031551

[7]   Ordaz, I., and Li, W., "Adaptive Aft Signature Shaping of a Low-Boom Supersonic Aircraft Using Off-Body Pressures," AIAA Paper 2012-20, January 2012. doi:10.2514/6.2012-20

[8]   Ordaz, I., Geiselhart, K., and Fenbert, J., "Conceptual Design of Low-Boom Aircraft with Flight Trim Requirement," *Journal of Aircraft*, Vol. 52, No. 3, 2015, pp. 932–939. doi:10.2514/1.C033160

[9]   Li, W., "Feasibility of Supersonic Aircraft Concepts for Low-Boom and Flight Trim Constraints," AIAA Paper 2015-2581, June 2015. doi:10.2514/6.2015-2581

[10] Ueno, A., Kanamori, M., and Makino, Y., "Multi-fidelity Low-boom Design Based on Near-field Pressure Signature," AIAA Paper 2016–2033, January 2016. doi:10.2514/6.2016-2033

[11] Aftosmis, M., Nemec, M., and Cliff, S., "Adjoint-Based Low-Boom Design with Cart3D," AIAA Paper 2011-3500, June 2011. doi:10.2514/6.2011-3500

[12] Wintzer, M., Ordaz, I., and Fenbert, J., "Under-Track CFD-Based Shape Optimization for a Low-Boom Demonstrator Concept," AIAA Paper 2015-2260, June 2015. doi:10.2514/6.2015-2260

[13] Mack, R., "A Supersonic Business-Jet Concept Designed for Low Sonic Boom," NASA TM-2003-212435, October 2003.

[14] Geiselhart, K., Ozoroski, L., Fenbert, J., Shields, E., and Li, W., "Integration of Multifidelity Multidisciplinary Computer Codes for Design and Analysis of Supersonic Aircraft," AIAA Paper 2011-0465, January 2011. doi:10.2514/6.2011-465

[15] Morgenstern, J., Norstrud, N., Stelmack, M., and Jha, P., "Advanced Concept Studies for Supersonic Commercial Transports Entering Service in 2030-2035 (N+3)," AIAA Paper 2010-5114, June 2010. doi:10.2514/6.2010-5114

[16] Morgenstern, J., Norstrud, N., Sokhey J., Martens, S., and Alonso, J., "Advanced Concept Studies for Supersonic Commercial Transports Entering Service in the 2018 to 2020 Period," NASA CR-2013-217820, February 2013.

[17] Welge, H., Bonet, J., Magee, T., Tompkins, D., Britt, T., Nelson, C., Miller, G., Stenson, D., Staubach, J., Bala, N., Duge, R., O'Brien, M., Cedoz, R., Barlow, A., Martins, S., Viars, P., Rasheed, A., Kirby, M., Raczynski, C., Roughen, K., Doyle, S., Alston, K., Page, J., and Plotkin, K., "N+3 Advanced Concept Studies for Supersonic Commercial Transport Aircraft Entering Service in the 2030-2035 Period," NASA CR-2011-217084, April 2011.

[18] Magee, T., Fink, L., Fugal, S., Adamson, E., and Shaw, S., "Boeing N+2 Supersonic Experimental Validation Phase II Program," AIAA Paper 2014-2137, June 2014. doi:10.2514/6.2014-2137

[19] Alonso, J., LeGresley, P., and Pereyra, V., "Aircraft Design Optimization," *Mathematics and Computers in Simulation*, Vol. 79, No. 6, 2009, pp. 1948–1958. doi:10.1016/j.matcom.2007.07.001

[20] Mathieu, M., Marin, A., Stephenson, K., Beard, J., Castillo, E., Weddle-Weaver, C., Teni, D., and Takahashi, T., "Preliminary Design of an N+1 Overwater Supersonic Commercial Transport Aircraft," AIAA Paper 2017-1387, June 2017. doi:10.2514/6.2017-1387

[21] Smith, H., "A Review of Supersonic Business Jet Design Issues," *The Aeronautical Journal*, Vol. 111, No. 1126, 2007, pp. 761–776. doi:10.1017/S0001924000001883

[22] Sun, Y., and Smith, H., "Review and Prospect of Supersonic Business Jet Design," *Progress in Aerospace Sciences*, Vol. 90, April 2017, pp. 12–38. doi:10.1016/j.paerosci.2016.12.003

[23] Alonso, J., and Colonno, M., "Multidisciplinary Optimization with Applications to Sonic-Boom Minimization," *Annual Review of Fluid Mechanics*, Vol. 44, January 2012, pp. 505–526. doi:10.1146/annurev-fluid-120710-101133

[24] Choi, S., Alonso, J., Kroo, I., and Wintzer, M., "Multifidelity Design Optimization of Low-Boom Supersonic Jets," AIAA Paper 2004-4371, August 2004. *Journal of Aircraft*, Vol. 45, No. 1, 2008, pp. 106–118. doi:10.2514/1.28948

[25] Furukawa, T., and Makino, Y., "Conceptual Design and Aerodynamic Optimization of Silent Supersonic Aircraft at JAXA," AIAA Paper 2007-4166, June 2007. doi:10.2514/6.2007-4166

[26] Makino, Y., "Low Sonic-Boom Design of a Silent Super Sonic Technology Demonstrator – Development of CAPAS and Its Application," *Proceedings of International Workshops on Numerical Simulation Technology for Design of Next Generation Supersonic Civil Transport*, JAXA Special Publication, 2007, pp. 697–704.

[27] Rallabhandi, S., and Mavris, D., "Aircraft Geometry Design and Optimization for Sonic Boom Reduction," *Journal of Aircraft*, Vol. 44, No. 1, 2007, pp. 35–47. doi:10.2514/1.20456

[28] Chiba, K., Makino, Y., and Takatoya, T., "Multidisciplinary Design Exploration of Wing Shape for Silent Supersonic Technology Demonstrator," AIAA Paper 2007-4167, June 2007. doi:10.2514/6.2007-4167

[29] Chiba, K., Makino, Y., and Takatoya, T., "Evolutionary-Based Multidisciplinary Design Exploration for Silent Supersonic Technology Demonstrator Wing," *Journal of Aircraft*, Vol. 45, No. 5, 2008, pp. 1481–1494. doi:10.2514/1.33272

[30] Deremaux, Y., Pietremont, N., Negrier, J., Herbin, E., and Ravachol, M., "Environmental MDO and Uncertainty Hybrid Approach Applied to a Supersonic Business Jet," AIAA Paper 2008-5832, September 2008. doi:10.2514/6.2008-5832

[31] Hamel, L., Folk, T., Jimenez, H., and Mavris, D., "Conceptual Design of an N+2 Supersonic Airliner," AIAA Paper 2009-7075, September 2009. doi:10.2514/6.2009-7075

[32] Kanazaki, M., Seto, N., and Jeong, S., "Knowledge Discovery for Multi-disciplinary Design of Silent Supersonic Transport Based on Efficient Global Optimization," *The 6th China-Japan-Korea Joint Symposium on Optimization of Structural and Mechanical Systems*, June 2010.

20

American Institute of Aeronautics and Astronautics

[33] Brezillon, J., Carrier, G., and Laban, M., "Multi-Disciplinary Optimization Including Environmental Aspects Applied to Supersonic Aircraft," The 7th ICAS Conference Proceedings, 2010.

[34] Brezillon, J., Carrier, G., and Laban, M., "Multidisciplinary Optimization of Supersonic Aircraft Including Low-Boom Considerations," *Journal of Mechanical Design*, Vol. 133, No. 10, 105001, October 2011. doi:10.1115/1.4004972

[35] Chiba, K., Makino, Y. and Takatoya, T., "Design-Informatics Approach for Intimate Configuration of Silent Supersonic Technology Demonstrator," *Journal of Aircraft*, Vol. 49, No. 5, 2012, pp.1200–1211. doi:10.2514/1.C031116

[36] Kanazaki, M., and Seto, N., "Efficient Global Optimization Applied to Design and Knowledge Discovery of Supersonic Wing," *Journal of Computational Science and Technology*, Vol. 6, No. 1, 2012, pp. 1–15.

[37] Yuhara, T. and Rinoie, K., "Conceptual Design Study on Low Boom LH2 Supersonic Transport for the 2030-2035 Time Frame," AIAA Paper 2012-23, January 2012. doi:10.2514/6.2012-23

[38] Salah el Din, I., Le Pape, L., M., Minelli, A., Grenon, R., and Carrier, G., "Impact of Multipole Matching Resolution on Supersonic Aircraft Sonic Boom Assessment," *Progress in Flight Physics*, Vol. 5, June 2013, pp. 601–620. doi: 10.1051/eucass/201305601

[39] Phillips, B., and West, T., "Trim Flight Conditions for a Low-Boom Aircraft Design Under Uncertainty," *Journal of Aircraft*, Vol. 56, No. 1, 2019, pp. 53–67. doi:10.2514/1.C034932

[40] Kasuga, Y., and Yoshida, K., "A New F-Function for the Low-Boom Aircraft Design with Trim Requirement," AIAA Paper 2016-2032, January 2016. doi:10.2514/6.2016-2032

[41] Minelli, A., Salah el Din, I., and Carrier, G., "Inverse Design Approach for Low-Boom Supersonic Configurations," *AIAA Journal*, Vol. 52, No. 10, 2014, pp. 2198–2212. doi:10.2514/1.J052834

[42] Mack, R., and Kuhn, N., "Determination of Extrapolation Distance with Measured Pressure Signatures from Two Low-Boom Models," NASA TM-2004-213264, November 2004.

[43] Makino, Y., Suzuki, K., Noguchi, M., and Yoshida, K., "Nonaxisymmetrical Fuselage Shape Modification for Drag Reduction of Low-Sonic-Boom Airplane," *AIAA Journal*, Vol. 41, No. 8, 2003, pp. 1413–1420. doi:10.2514/2.2109

[44] Martins, J., and Lambe, A., "Multidisciplinary Design Optimization: a Survey of Architectures," *AIAA journal*, Vol. 51, No. 9, 2013. pp. 2049–2075. doi:10.2514/1.J051895

[45] OpenVSP, Version 3.21.1, Open Source, URL:http://www.openvsp.org [retrieved 9 July 2020].

[46] Candel, S., "Concorde and the Future of Supersonic Transport," *Journal of Propulsion and Power*, Vol. 20, No. 1, 2004, pp. 59–68. doi:10.2514/1.9180

[47] Ladson, C., Brooks, C., Jr., Hill, A., and Sproles, D., "Computer Program to Obtain Ordinates for NACA Airfoils," NASA TM-1996-4741, December 1996.

[48] Li, W. and Shields, E., "Generation of Parametric Equivalent-Area Targets for Design of Low-Boom Supersonic Concepts," AIAA Paper 2011-462, January 2011. doi:10.2514/6.2011-462

[49] Ozoroski, L., Geiselhart, K., Padula, S., Li, W., Olson, E., and Campbell, R., "Initial Multidisciplinary Design and Analysis Framework," NASA TM-2010-216711, June 2010.

[50] Lytle, J., "The Numerical Propulsion System Simulation: An Overview," NASA/TM-2000-209915, June 2000.

[51] Numerical Propulsion System Simulation (NPSS), Version 2.8, Southwest Research Institute, URL:https://www.swri.org/consortia/numerical-propulsion-system-simulation-npss [retrieved 9 June 2020].

[52] Mccullers, L., "FLOPS User Guide," NASA Langley Research Center, Hampton, Virginia, 2008 (available with public distribution of software).

[53] McCullers, L., and Linwood, A., "FLOPS Takeoff and Landing Module Documentation. FLOPS Users Manual," NASA Langley Research Center, Hampton, Virginia, 2008 (available with public distribution of software).

[54] Carlson, H., Chu, J., Ozoroski, L., and McCullers, L., "Guide to AERO2S and WINGDES Computer Codes for Prediction and Minimization of Drag Due to Lift," NASA TP-3637, November 1997.

[55] Sommer, S., and Short, B., "Free-Flight Measurements of Turbulent-Boundary-Layer Skin Friction in the Presence of Severe Aerodynamic Heating at Mach Numbers from 2.8 to 7.0," NACA TN-3391, 1955.

[56] Harris, R., Jr., "An Analysis and Correlation of Aircraft Wave Drag," NASA TM X-947, March 1964.

[57] Wells, D., Horvath, B., and McCullers, L., "The Flight Optimization System Weights Estimation Method," NASA TM-2017-219627, Volume 1, January 2017.

[58] Rallabhandi, S., "Advanced Sonic Boom Prediction Using Augmented Burgers Equation," *Journal of Aircraft*, Vol. 48, No. 4, 2011, pp. 1245–1253. doi:10.2514/1.C031248

[59] Shepherd, K., and Sullivan, B., "A Loudness Calculation Procedure Applied to Shaped Sonic Booms," NASA TP-3134, November 1991.

[60] Carlson, H., and Mack, R., "Estimation of Wing Nonlinear Aerodynamic Characteristics at Supersonic Speeds," NASA TP-1718, November 1980.

[61] Li, W., Geiselhart, K., Olson, E., and Robinson, J., "Automation of Structural Sizing of Aircraft Concepts Under Static Aeroelastic Constraints," AIAA Paper 2018-0103, January 2018. doi:10.2514/6.2018-0103

[62] Tseng, P., "Convergence of a Block Coordinate Descent Method for Nondifferentiable Minimization," *Journal of Optimization Theory and Applications*, Vol. 109, No. 3, 2001, pp. 475–494. doi:10.1023/A:1017501703105

[63] ModelCenter, Version 12.0, Phoenix Integration Inc., URL:http://www.phoenix-int.com [retrieved 9 July 2020].

[64] Uber eVTOL common reference models, URL:https://www.uber.com/us/en/elevate/uberair/ [retrieved 9 July 2020].